THE REPUBLIC OF TURKEY
BAHÇEŞEHİR UNIVERSITY

COMPUTATIONAL FLUID DYNAMICS ANALYSIS OF A QUADROTOR

Master Thesis

BURAK SUNAN

ISTANBUL, 2014

THE REPUBLIC OF TURKEY
BAHÇEŞEHİR UNIVERSITY

THE GRADUATE SCHOOL OF NATURAL AND APPLIED SCIENCES

M.S. MECHATRONICS ENGINEERING

COMPUTATIONAL FLUID DYNAMICS ANALYSIS OF A QUADROTOR

Master Thesis

BURAK SUNAN

Supervisor: Prof. Dr. Oktay OZCAN

ISTANBUL, JANUARY 2014

THE REPUBLIC OF TURKEY
BAHÇEŞEHIR UNIVERSITY

THE GRADUATE SCHOOL OF NATURAL AND APPLIED SCIENCES

M.S. MECHATRONICS ENGINEERING

Name of the thesis: **Computational Fluid Dynamics Analysis of a Quadrotor**

Name/Last Name of the Student: **Burak SUNAN**
Date of the Defense of Thesis: **15.01.2014**

The thesis has been approved by the Graduate School of Natural and Applied Sciences.

Doç. Dr. Tunç BOZBURA
Graduate School Director

I certify that this thesis meets all the requirements as a thesis for the degree of Master of Science.

Prof. Dr. Oktay OZCAN
Program Coordinator

This is to certify that we have read this thesis and we find it fully adequate in scope, quality and content, as a thesis for the degree of Master of Science.

Examining Committee Members	Signature
Thesis Supervisor Prof. Dr. Oktay OZCAN	----------
Member Yrd. Doç. Dr. Berke GÜR	----------
Member Prof. Dr. Mehmet Barış ÖZERDEM	----------

ABSTRACT

COMPUTATIONAL FLUID DYNAMICS ANALYSIS OF A QUADROTOR

Burak SUNAN

M. Sc. Mechatronics Engineering

Thesis Supervisor: Prof. Dr. Oktay OZCAN

January, 2014, 68 pages

Quadrotor, which is capable of VTOL (Vertical Take-off and Landing) by means of four propellers, is a commonly used UAV (Unmanned Aerial Vehicle) for lifting loads, civil or military observations and also entertainment. Various quadrotor types are available, for instance remotely controlled devices for lifting, civil observations and entertainment and autonomous controlled quadrotors for military services.

There are many studies on how to control VTOL UAVs. The most remarkable issue is the determination of lift, thrust and drag forces. These forces are measured via experimental platforms, thus the static forces can only be determined with these types of platforms. The measurements of dynamic forces on UAVs are really difficult.

However, CFD (Computational Fluid Dynamics) analyses make the dynamic force determination easier. Not only lift and drag forces on propellers but also the aerodynamics effects on quadrotor body can be simulated with suitable CFD processes. The aim of the present study is to analyze a quadrotor via CFD and determine the aerodynamics behavior of a quadrotor.

Keywords: CFD, Quadrotor, Propeller, Aerodynamics, Lift, Drag, Thrust

ÖZET

QUADROTOR HESAPLAMALI AKIŞKANLAR DİNAMİĞİ ANALİZİ

Burak SUNAN

Mekatronik Mühendisliği Yüksek Lisans Programı

Tez Danışmanı: Prof. Dr. Oktay OZCAN

Ocak, 2014, 68 sayfa

Quadrotor, 4 rotor vasıtasıyla VTOL (dikey iniş ve kalkış) kapasitesine sahip, genel olarak yük kaldırma, sivil ve askeri gözlemler ve eğlence için kullanılan IHA (insansız hava aracı) türüdür. Eğlence, yük kaldırma ve sivil uygulamalar için uzaktan kontrollü veya askeri uygulamalar için otonom kontrollü çeşitli quadrotorlar dizayn edilmiştir.

VTOL İHA'ların kontrolleri ile ilgili çeşitli araştırmalar ve deneyler yapılmaktadır. En dikkat edilmesi gereken konu ise kaldırma, sürtünme ve itki kuvvetlerinin ölçümleridir. Bu kuvvetler deneysel platform vasıtası ile ölçülebilir, aslında sadece statik kuvvetler bu tip platformlar sayesinde hesaplanabilir. Dinamik kuvvetlerin ölçümleri oldukça zordur.

Ancak, CFD (Hesaplanmalı Akışkanlar Dinamiği) analizleri dinamik kuvvetlerin ölçümlerini kolaylaştırır. Sadece kaldırma ve sürtünme kuvvetlerini değil, quadrotor üzerindeki aerodinamik efektleri de doğru CFD süreçleri ile hesaplanabilir ve simule edilebilir.

Anahtar Kelimeler: CFD, Quadrotor, Pervane, Aerodinamik, Kaldırma, Sürtünme, İtki

CONTENTS

TABLES

FIGURES

ABBREVIATIONS

BC	:	Boundary Condition
CFD	:	Computational Fluid Dynamics
DM	:	Design Modeler
FEM	:	Finite Element Method
MRF	:	Multiple Reference Frame
SIMPLE	:	Semi-Implicit Method for Pressure-Linked Equations
UAV	:	Unmanned Aerial Vehicle
VTOL	:	Vertical Take-Off and Landing

SYMBOLS

rpm	:	revolution per second
m/s	:	meter per second
M	:	Mach number
N	:	Newton

1. INTRODUCTION

1.1 BACKGROUND

A quadrotor, also called quadcopter, is a type of multicopter with four rotors and a commonly used UAV (Unmanned Aerial Vehicle) for civil or military observations. VTOL (Vertical Take-Off and Landing) is a popular research area and various designs have been produced for the purpose of aerial photography, air-shipping for short distances, entertainment, military observations and etc. The quadrotor studied in this thesis is shown in Figure 1.1.

Figure 1.1: A Model Quadrotor

Source: http://grabcad.com/library/waterproof-quadrotor

VTOL UAVs is the best choice for many military or civil purposes, saving valuable time for people, compared to aircrafts. There are many studies and experiments on how to control VTOL UAVs. In addition, quadrotors have strong maneuverability by means of four rotors, thus control algorithms of quadrotors are complicated in order to overcome aerodynamic instabilities.

A significant issue is the determination of lift and drag forces in order to control unwanted disturbances. Electronically, the speed of rotor can be controlled, however the thrust force doesn't just depend on rotor speed, but it also depends on propeller dimensions and geometry.

Thrust, lift, and drag forces can be measured by experiments, thus the static forces on a rotor can only be determined with these experiments. However, the measurements of

dynamic forces on UAVs are really difficult. The experiments for determination of dynamic forces can be accomplished with large costs.

On the other hand, CFD (Computational Fluid Dynamics) analyses make the determination of dynamic force easier. All aerodynamics effects on the quadrotor body can examined with suitable a CFD methodology. Therefore, the aim of the present thesis is to analyze a quadrotor by CFD and find its aerodynamics behavior.

Figure 1.2: Computational Fluid Dynamics

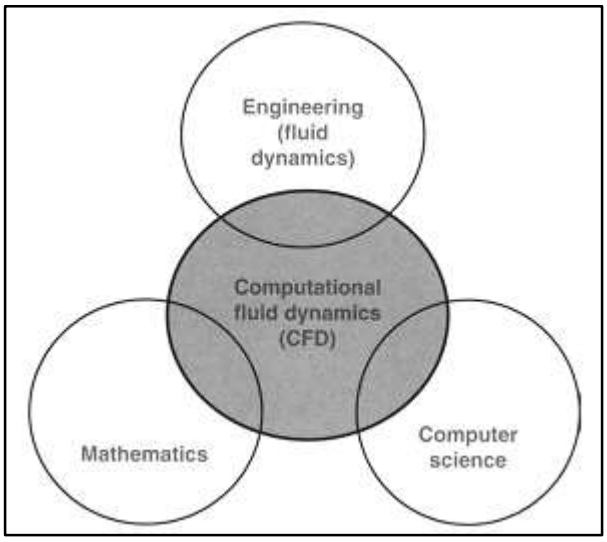

Source: (Tu and others 2007, p. 2)

CFD is the analysis of systems involving fluid flow, heat transfer and associated phenomena such as chemical reactions by means of computer-based simulation. The technique is very powerful and spans a wide range of industrial and non-industrial application areas. Some examples are: (Versteeg & Malalasekera 1995, p. 1)

i. Aerodynamics of aircraft and vehicles: lift and drag
ii. Hydrodynamics of ships
iii. Power plant: combustion in IC engines and gas turbines
iv. Turbomachinery: flows inside rotating passages, diffusers etc.
v. Electrical and electronic engineering: cooling of equipment including microcircuits
vi. Chemical process engineering: mixing and separation, polymer moulding
vii. External and internal environment of buildings: wind loading and heating / ventilation

viii. Marine engineering: loads on off-shore structures

ix. Environmental engineering: distribution of pollutants and effluents

x. Hydrology and oceanography: flows in rivers, estuaries, oceans

xi. Meteorology: weather prediction

xii. Biomedical engineering: blood flows through arteries and vein

CFD has certainly become a new branch integrating not only the disciplines of fluid mechanics with mathematics but also with computer science as illustrated in Figure 1.2. (Tu and others 2007, p. 2)

Figure 1.3: Vortex wake of UH-60 rotor of Blackhawk Helicopter

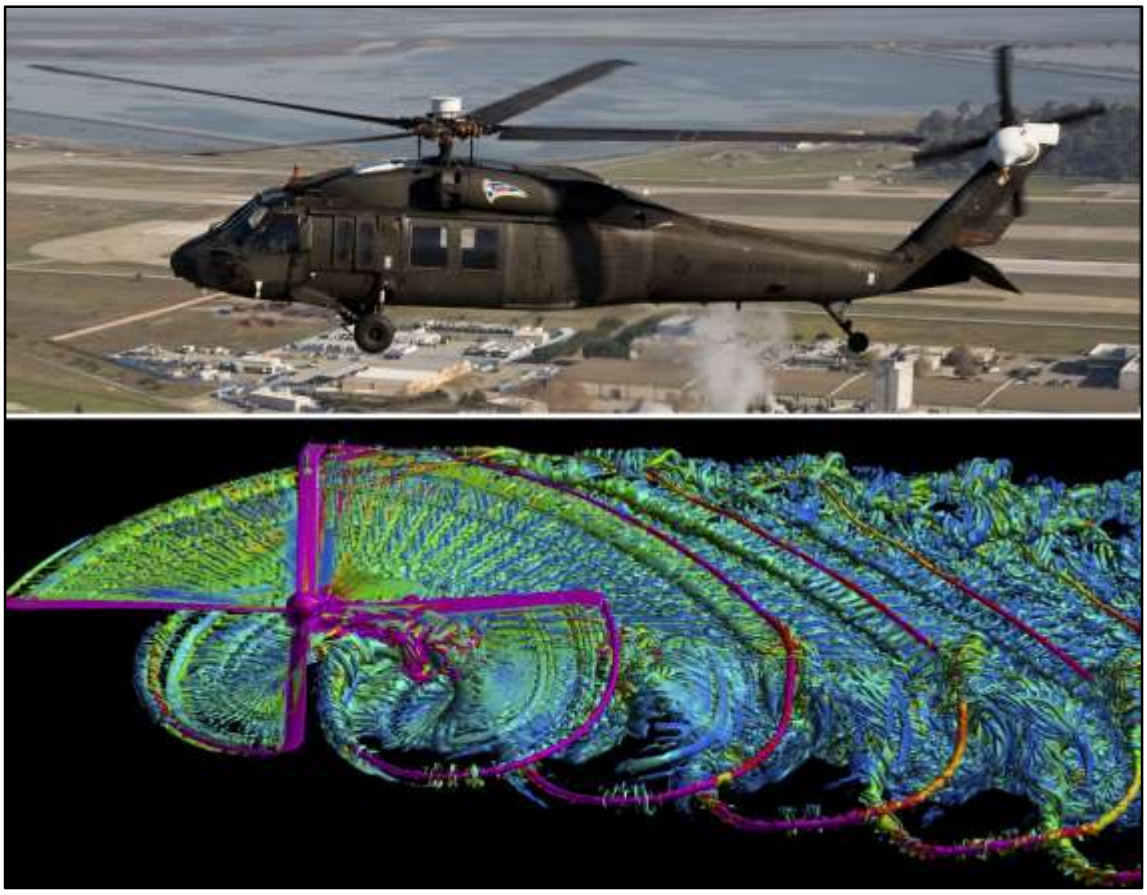

Source: http://www.nas.nasa.gov/SC12/assets/images/content/Chaderjian_N_Blachawk_1.jpg

Aerodynamics is the study of relative flow of air past an aircraft or any other object of interest like train, automobile, building etc. There are 3 components in modern aerodynamics studies. These are experimental, theoretical and CFD approaches respectively. Experimental studies are conducted in wind tunnels. Wind tunnels are used

to perform aerodynamic measurement on scaled down models of prototypes. The main disadvantages of experimental approach are high capital and running cost of wind tunnels, skill required in manufacturing models accurately and in acquisition of data, interpretation of data etc. Theoretical and CFD studies have led to valuable understanding of wide range of flow problems. (Roy 2012, p. 6-7)

For instance, in Figure 1.3, time-dependent tip vortices and the vortex wake are provided by CFD. Magenta and blue colors correspond to high and low values of vorticity, respectively. Vorticity is the curl of velocity in a velocity field and one of the most powerful quantities in theoretical aerodynamics. (Anderson 2001, p. 141-145)

Figure 1.4: The predicted ground plane surface flow for a UH-60

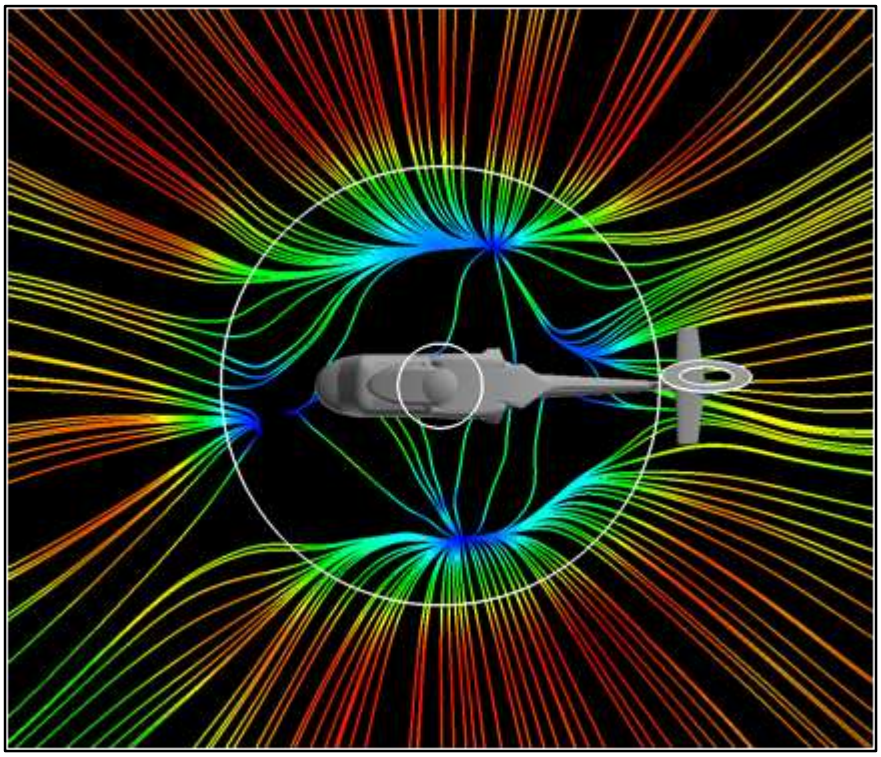

Source: http://rotorcraft.arc.nasa.gov/Research/Programs/brownout.html

The fluid variables, not just vorticity, also drag, lift and thrust forces, pressure, velocity, density and temperature etc., can determined by CFD and presented in colorful plots. Thus, CFD is also expressed sarcastically as Colorful Fluid Dynamics. Another example, in Figure 1.4, the ground effect of a UH-60 helicopter is rendered by wall shear magnitude.

CFD is playing a crucial role in overcoming many challenges faced by aerospace and defense industries in improving flight and in solving a diverse array of designs. Today, CFD is being applied to many more difficult operational problems that were too unwieldy to analyze or solve with computational tools in the past. (Tu and others 2007, p. 9-10)

Table 1.1: The commercial CFD programs list

6sigmaDC	COMSOL Multiphysics CFD Module	FLUENT	PumpLinx
Applied Computational Fluid Dynamics	Coolit	FLUIDYN	Range Software
AcuSolve	CoolitPCB	FluSol	RheoChart
ADINA - F	DLR - TAU	GASP	scSTREAM
ADINA - FSI	DQMoM	HeatDesigner	SC/Tetra
ANANAS	EasyCFD	J - FLO	Siemens PLM Software CFD
ANSWER	FENSAP - ICE	Kameleon FireEx - KFX	Smartfire
Azore	FINE/Hexa	KINetics Reactive Flows	Solution of Boltzmann Equation
CFD++	FINE/Turbo	KIVA	SPLASH
CFD2000	FIRE	NOGRID	srm suite
CFD - FASTRAN	FLACS	NX Electronic Systems Cooling	STALLION 3D
CFD - ACE	FloEFD	NX Advanced Flow	STAR - CD
CFdesign	FloTHERM	NX Flow	STAR - CCM+
CFX	FloVENT	MicroFlo	Tdyn
CharLES	FLOW - 3D	PHOENICS	TMG - Flow
CONVERGE	FLOWVISION	PHYSICA	Turb'Flow
COMSOL Multiphysics	Flowz	PowerFLOW	TURBOcfd

Source: http://www.cfd-online.com/Wiki/Codes

1.2 OBJECTIVE

In CFD world, there are many researchers who develop their own codes, and also commercial codes which are being developed according to the industry needs. The commercial CFD programs in all around the world is listed in Table 1.1. Each cell of the table represents a commercial CFD code. One of the commercial software, is chosen companies in a wide variety of industry, is ANSYS Fluent, and in this research, over 20 CFD analyses of a model quadrotor are performed by ANSYS Fluent.

Figure 1.5: A MRF case in steady time of ANSYS Fluent

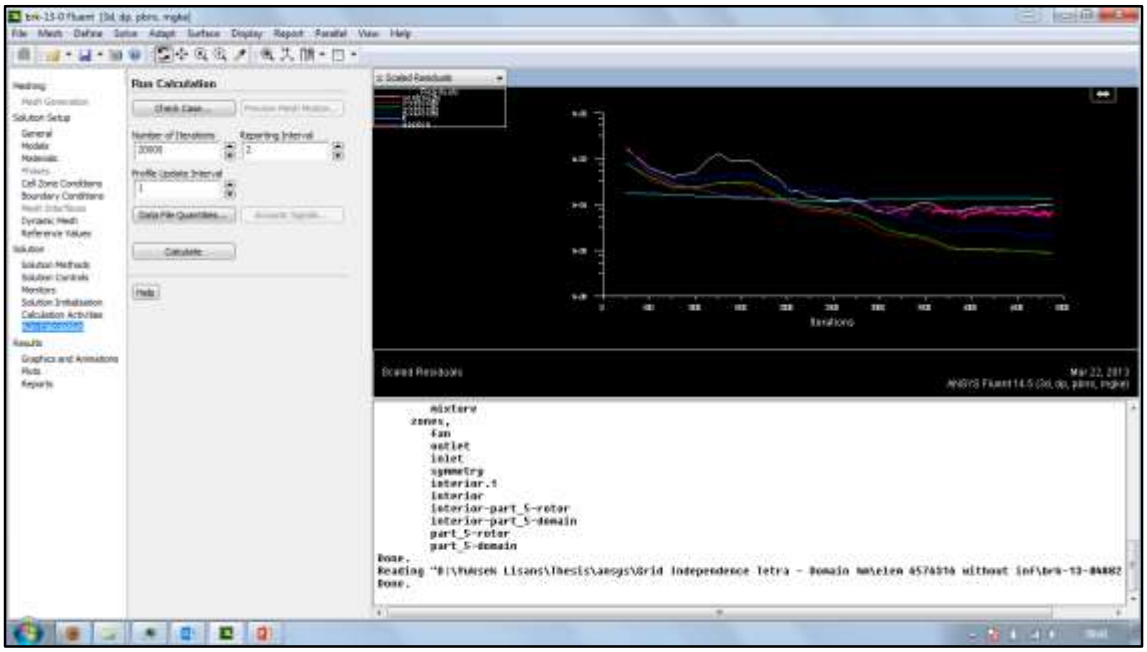

Source: a screenshot from ANSYS Fluent, captured for this research

This research presents an analysis of the aerodynamics characteristics of a quadrotor for both steady and unsteady flows. For steady flow cases, aerodynamics behaviour can be processed easily for many aerial vehicles in experimental platforms. However, unsteady flow conditions in experimental platforms make aerodynamics characterizations difficult, long term and many expensive. This study describes determination of lift, drag and thrust forces on the model quadrotor by ANSYS Fluent. A screenshot of Fluent is shown in Figure 1.5.

A significant issue is to find a CFD solution at hover position of the quadrotor. After getting sufficiently close agreement with some benchmarking experiments, the CFD methodology can be performed for more complicated geometries. The results of the study reveals the dynamics characteristics of a quadrotor. This demonstrates feasibility of designing a quadrotor by CFD which saves time and cost compared to experiments.

2. LITERATURE SEARCH

2.1 PROPELLER PERFORMANCE DATA AT LOW REYNOLDS NUMBERS

Brandt and Selig (2011) test totally 79 propellers are fit in 200 to 280 mm diameter range in the subsonic wind tunnel of UIUC (University of Illinois at Urbana-Campaign). All propellers are tested in the range 1500 rpm to 7500 rpm in order to examine Reynolds number effects. The objective is the selection proper propeller for UAVs can have a dramatic effect on aircraft performance.

Figure 2.1: The subsonic wind tunnel of UIUC

Source: (Brandt and Selig, p. 2)

Brandt and Selig (2011) collect many propeller with all specifications and also their geometry information on their web site. In this meeting paper, what they have done is explained sufficiently. Figure 2.1 indicates the subsonic wind tunnel of UIUC and Figure 2.2 shows the propeller is analyzed in this study is the geometry plot of APC Slow-Flyer 10x4.7. The propeller geometry is explained in Section 3.1 in more detail. In addition, Table 2.1 defines Figure 2.2 in more understandable.

Figure 2.2: APC Slow Flyer 10x4.7 geometry

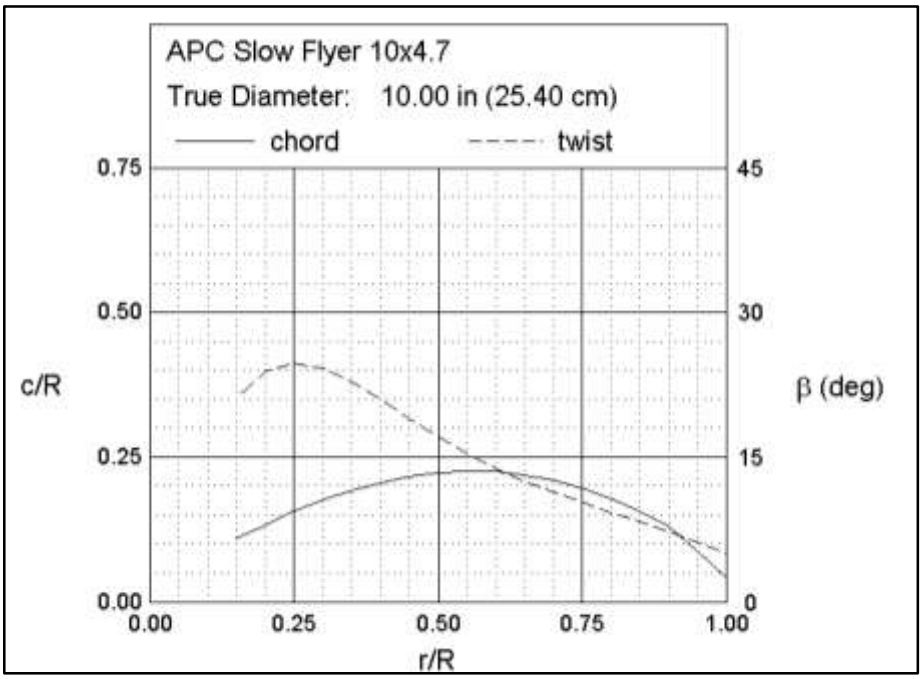

Source: http://aerospace.illinois.edu/m-selig/props/plots/apcsf_10x4.7_geom.png

Table 2.1: APC Slow Flyer 10x4.7 Geometry Data

r/R	c/R	beta
0.15	0.109	21.11
0.20	0.132	23.90
0.25	0.156	24.65
0.30	0.176	24.11
0.35	0.193	22.78
0.40	0.206	21.01
0.45	0.216	19.00
0.50	0.223	17.06
0.55	0.226	15.33
0.60	0.225	13.82
0.65	0.219	12.51
0.70	0.210	11.36
0.75	0.197	10.27
0.80	0.179	9.32
0.90	0.130	7.27
0.95	0.087	6.15
1.00	0.042	5.04

Source: http://aerospace.illinois.edu/m-selig/props/data/apcsf_10x4.7_geom.txt

3. MATERIALS & METHODS

3.1 QUADROTOR GEOMETRY

The chosen quadrotor with dimensions is represented in Figure 3.1 and all parts are downloaded from specified source. The weight of this quadrotor is approximately 1 kg. The propellers are APC Slow Flyer 10x4.7. APC is one the biggest model airplane propellers manufacturer and also APC propellers are commonly preferred by people interested in model airplanes and multicopters.

Figure 3.1: The Quadrotor Geometry with Dimensions

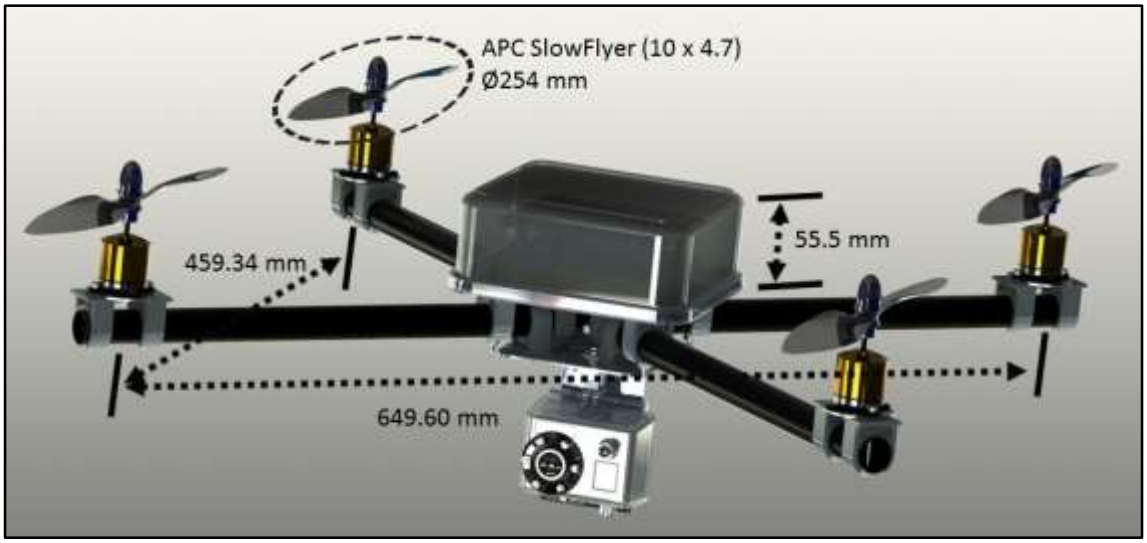

Source: https://grabcad.com/library/waterproof-quadrotor

The propeller length in inches is represented by first part of model number and second number represents the pitch distance in inches. In other words, APC Slow Flyer 10x4.7 generates 254 mm diameter actuator disc and 119.38 mm pitch length. In Figure 3.2, the pitch distance at wake is more understandable.

Figure 3.2: Pitch Distance Difference

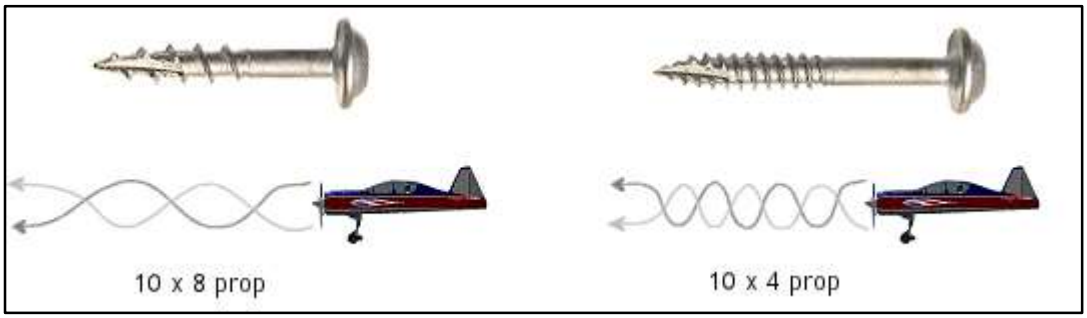

Source: http://www.rc-airplane-world.com/propeller-size.html

3.2 CFD METHODOLOGY

CFD is comprised of fluid mechanics theory and computational solutions practice. The practical side of CFD shares the same fundamental significance of theoretical side, thus it can be reached to the required level of CFD knowledge in order to make an effort on flow processes better. (Tu and others 2007, p. 30)

There are many shareware or freeware CFD codes and also commercial CFD packages. In addition, they can overcome many various flow problems with both structured and unstructured meshes and robust numerical algorithms. These programs have 3 parts; pre-processor, solver and post-processor, illustrated in Figure 3.3.

Figure 3.3: The inter-connectivity functions of three main parts of CFD

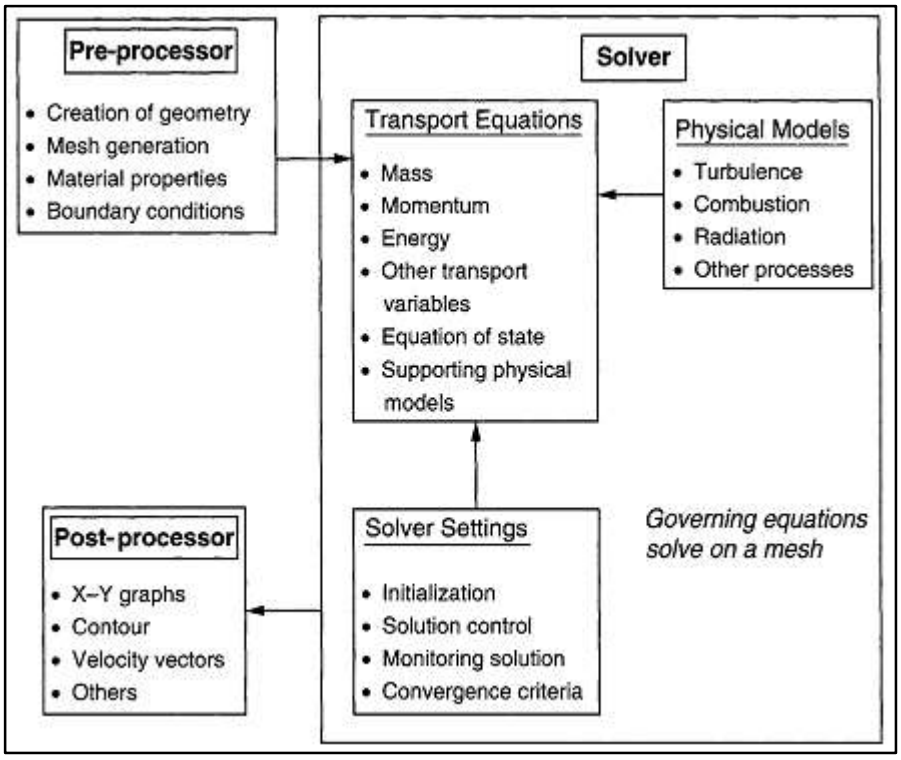

Source: (Tu and others 2007, p. 31)

3.2.1 Problem Setup – Pre-process

In pre-processor part, the problem setup is prepared properly with necessary steps. These steps are firstly geometric creation of computational domain, mesh (grid) generation, specification of fluid properties, and lastly boundary conditions.

3.2.1.1 Geometry of computational domain

The first step in any CFD analyses is the definition of geometry of the computational domain (i.e., the flow region, the control volume). All CFD problems have their own different control volumes. For instance, the inlet parts of the control volumes of inflow cases (i.e., internal flow, flow in a tube) should be sufficiently long so that the software can use uniform flow at inlet. The uniform flow can move through entrance length much longer and the uniform flow turns into the fully-developed flow, as shown in Figure 3.4. Therefore, CFD solutions of inflow cases give more accurate results if the boundary conditions reflects true physics.

Figure 3.4: Fully-developed flow

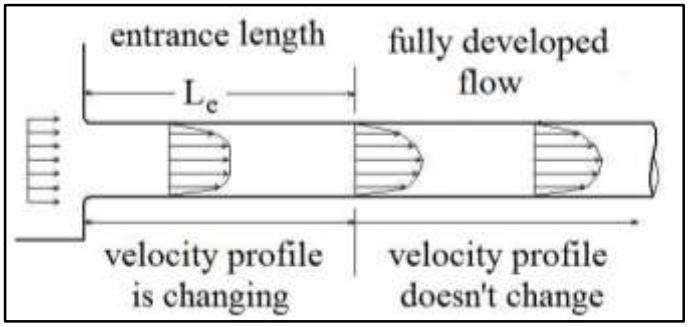

Source: http://www.brighthubengineering.com/hydraulics-civil-engineering/55543-pipe-flow-calculations-1-the-entrance-length-for-fully-developed-flow/

On the other hand, the outflow cases (i.e., external flow) can be solved with uniform flows, not fully-developed flow. In addition, the control volume shape can change according to the problem. For instance, the cylinder control volume is suitable for outflow fan cases. Moreover, airfoil cases are suitable with both rectangular domain and C-grid domain, as shown in Figure 3.5.

Figure 3.5: C-grid domain

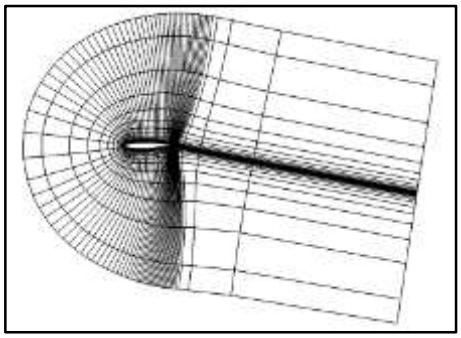

Source: http://www.cfd-online.com/Forums/star-ccm/75804-c-grid-around-airfoil.html

In this thesis, the control volume is generated as a quarter cylinder since each propellers on quadrotor are the same brand and have the same properties. It is sufficient to analyze one of them in order to gain fundamental knowledge for this research. In Figure 3.6, an estimated computational domain is drawn by ANSYS DM (Design Modeler) in order to show the control volume with quadrotor itself.

Figure 3.6: The quarter cylinder as an estimated control volume

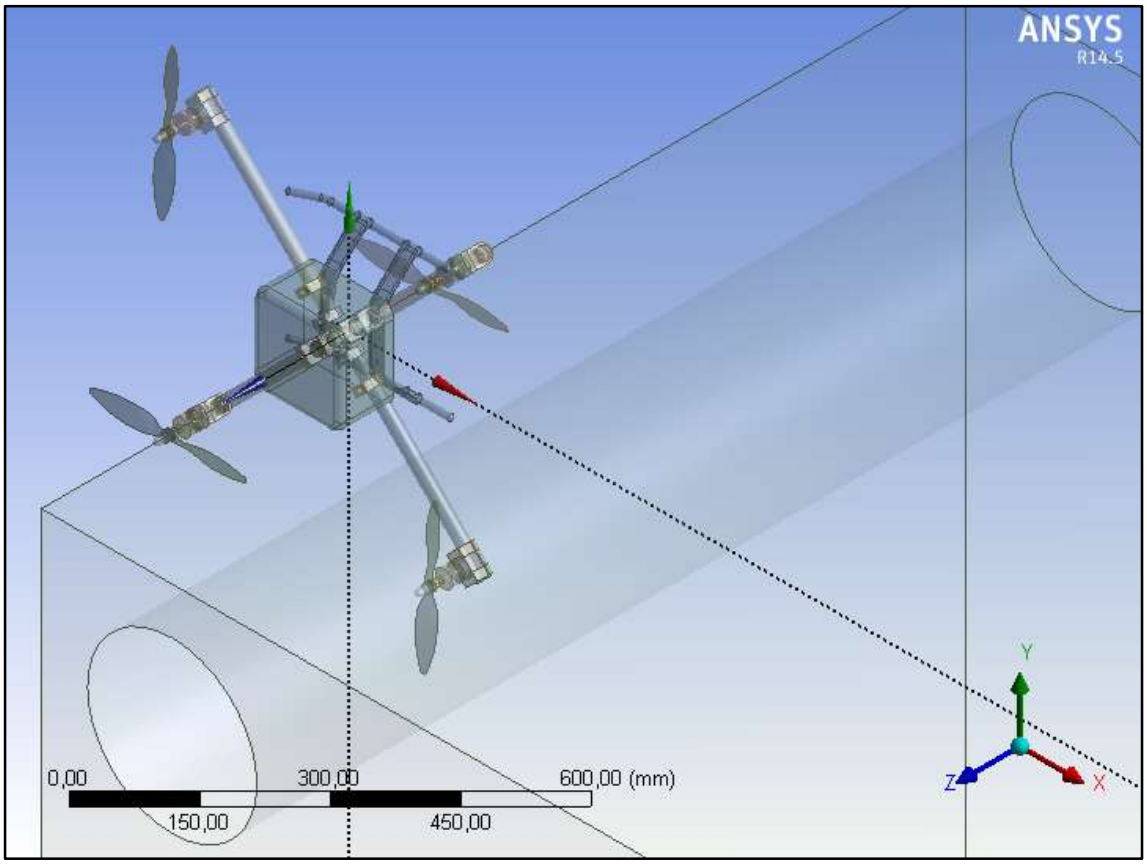

Source: a screenshot from ANSYS Design Modeler, captured for this research

The center of quarter cylinder is also the center of quadrotor. In addition, the small cylinder inside the quarter cylinder is related to rotor and covers the rotor totally. Thus, the rotor domain is created with the appropriate diameter which is 1.1 times larger than propeller length. The rotor domain is generated for rotating movement and the quarter cylinder domain remains the stationary domain, as illustrated in Figure 3.7.

As a result, the computational domain includes 2 zones; one of them can rotate with the propeller towards the propeller rotation direction, the other one always remains

stationary. This method is called MRF (Multiple Reference Frame), is commonly used for propeller, rotor and fan cases.

The diameter of the rotor domain is specified with D = 275 mm (1.1 times larger than propeller length). However, 2 different the stationary domains are described and also illustrated in Figure 3.7.

Two solution domains (long and short) have been used. Firstly, the long solution has a length that 80 times larger than propeller. The entrance length is 20D (5 m) and the output length is 36D (10 m) approximately. Thus, the long stationary domain has a total length of 15 m.

Secondly, the short domain is determined with 16 times larger than propeller length. The entrance length is 4D (1 m) and the output length is 12D (3 m) long approximately. Therefore, the short stationary domain has a total length of 4 m.

Figure 3.7: The control volume with distances

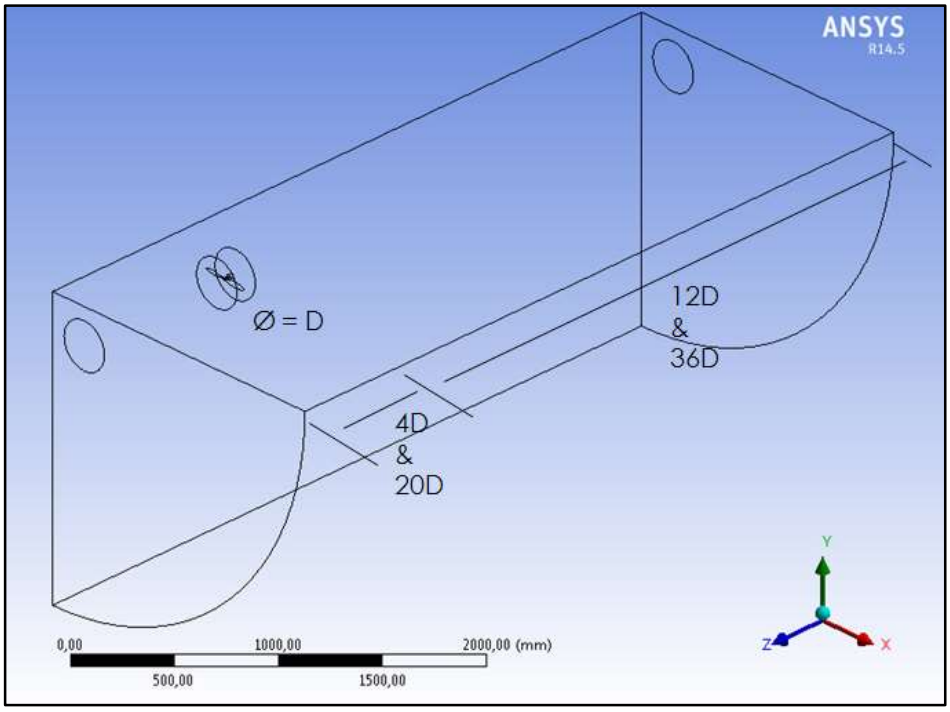

Source: a screenshot from ANSYS Design Modeler, captured for this research

The computation of the long domain needs a more powerful computer since the long domain has more cell number if the cell sizes of both the long and the short domains are

equal to each other approximately. If the long domain cell number is almost equal to the short one, the cell size of the long domain will be larger.

Thus, less accurate results are obtained from the long domain. In this research, both domains are calculated and compared and the compared solutions are obtained in Results.

3.2.1.2 Mesh generation

The second step is mesh (i.e., grid) generation constitutes the most critical situation during all CFD processes. CFD needs to divide smaller pieces to computational domain in order to solve flow physics. If the solution domain is separated to so many parts, the more accurate results will be obtained. This small divided elements are called "the cells of mesh or grid" in CFD literature.

The necessary flow is determined with each cell is numerically solved and these solved cells give consequences with primitive variables such as velocity, pressure, temperature, density, specific heat and etc.

Figure 3.8: The difference between the structured and unstructured mesh

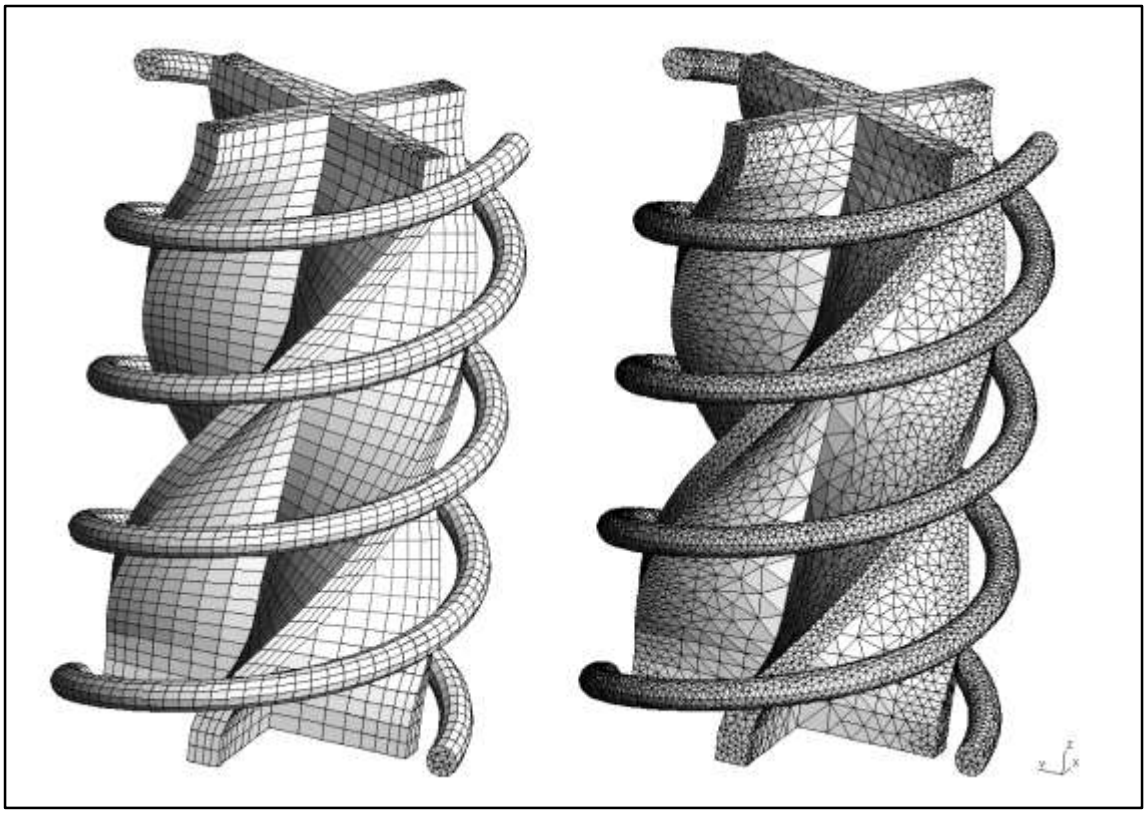

Source: http://geuz.org/gmsh/gallery/spirale.gif

The accurate results are not just depend on element number of grid, the mesh type can be increased in variety according to the computational domain shapes. For instance, simple control volumes can be meshed with structured grid. However, the computational domains with complicated shapes can be meshed with unstructured grid. The structured grid is generated with logical representation otherwise the unstructured grid is placed with arbitrary representation. The difference between them is illustrated in Figure 3.8.

In this research, the stationary domain has a quarter cylinder shape and it can be meshed with structured mesh easily. However, although the rotor domain seems totally cylinder, it has also propeller with a twisted shape. Thus, the structured mesh seems so difficult in the rotor domain and the unstructured mesh overlays the rotor domain. Both domain mesh are shown in Figure 3.9.

Figure 3.9: Structured mesh on stationary and unstructured mesh on rotor domains

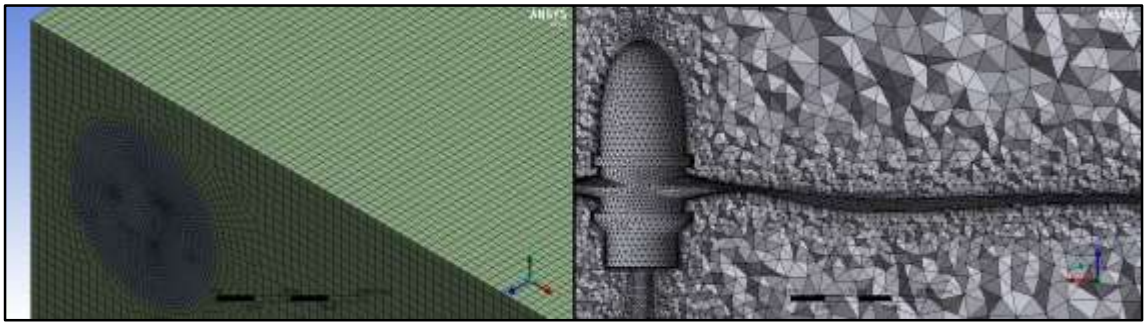

Source: a screenshot from ANSYS Workbench Meshing, captured for this research

The flow separation on propeller surface should be predicted in order to obtain the drag and lift forces more accurately. The unstructured mesh gives less accurate results than the structured mesh but on the propeller surface, the prismatic mesh type is chosen to get better results.

The prismatic mesh type is produced for complex geometries in order to get more efficient results. The prismatic mesh layers are placed with inflation method by ANSYS Workbench Meshing supports all mesh type smoothly. The prismatic mesh firstly looks like unstructured grid but it can be laid logically. The first prismatic layer must be the smallest because of near-wall approximation and each layer gets larger with a grow rate, is illustrated in Figure 3.10.

Figure 3.10: The prismatic layer mesh type on propeller surface

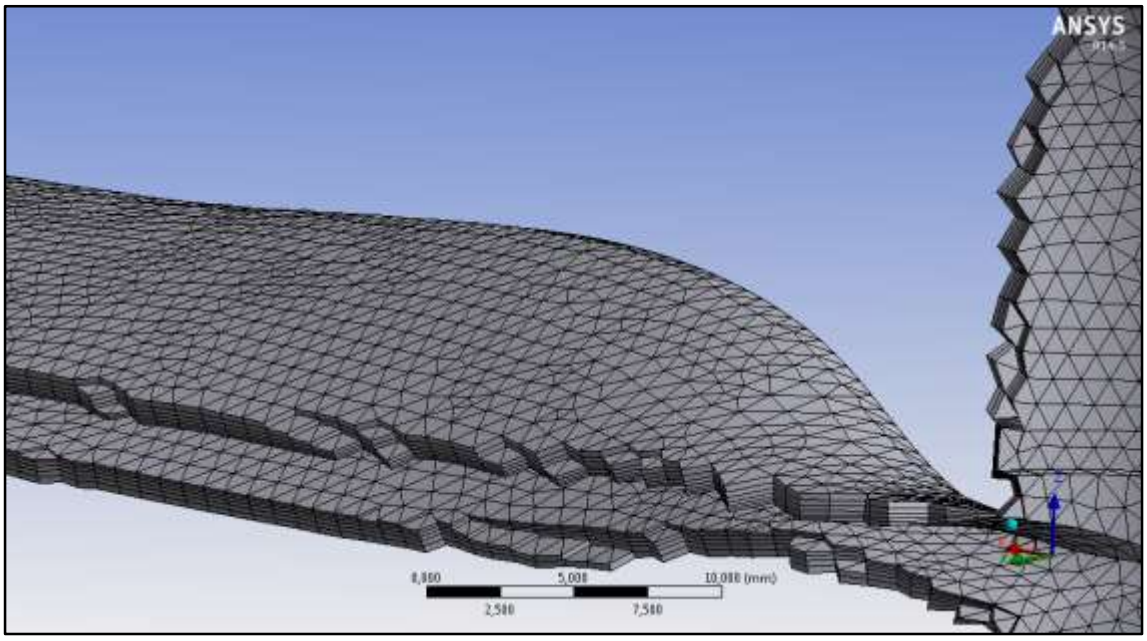

Source: a screenshot from ANSYS Workbench Meshing, captured for this research

3.2.1.3 Physics and fluid properties

Many industrial CFD problems need satisfactory results for their complex flow processes. For instance, complicated chemical reactions in combustion chambers, hypersonic flow problems in defense industry or re-entry issues for space shuttles. In addition, combustion problems also require radiation models.

The choice of physics model is the third important step after geometry creation and mesh generation. Various physics model in CFD is generated according to the problems such as compressible and incompressible flows, heat transfer and radiation, non-linear problems, acoustics, chemical problems, subsonic – hypersonic flows and etc.

Moreover, some physics models can be solved their own mesh style. In Figure 3.11, from Tu and others 2007, p. 38, below the main banner of "Computational Fluid Dynamics & Heat Transfer", various flow physics are illustrated with problem samples. The physics model in CFD should be identified carefully and its necessary should be determined in detail.

In this research, the turbulence viscous model is chosen and the incompressible flow with external domain is solved since the propeller can resist max 7500 rpm because of its

material. Thus, the tip speed on the propeller is equal to 99.75 m/s and the Mach number is 0.29 M which is lower than 0.7 M. That means the subsonic flow or the low speed air occurs around the propeller. In addition, approximately 20 different cases are run in both steady and unsteady time and the solutions are discussed in the Results section.

Figure 3.11: A flowchart encapsulating the various flow physics in CFD

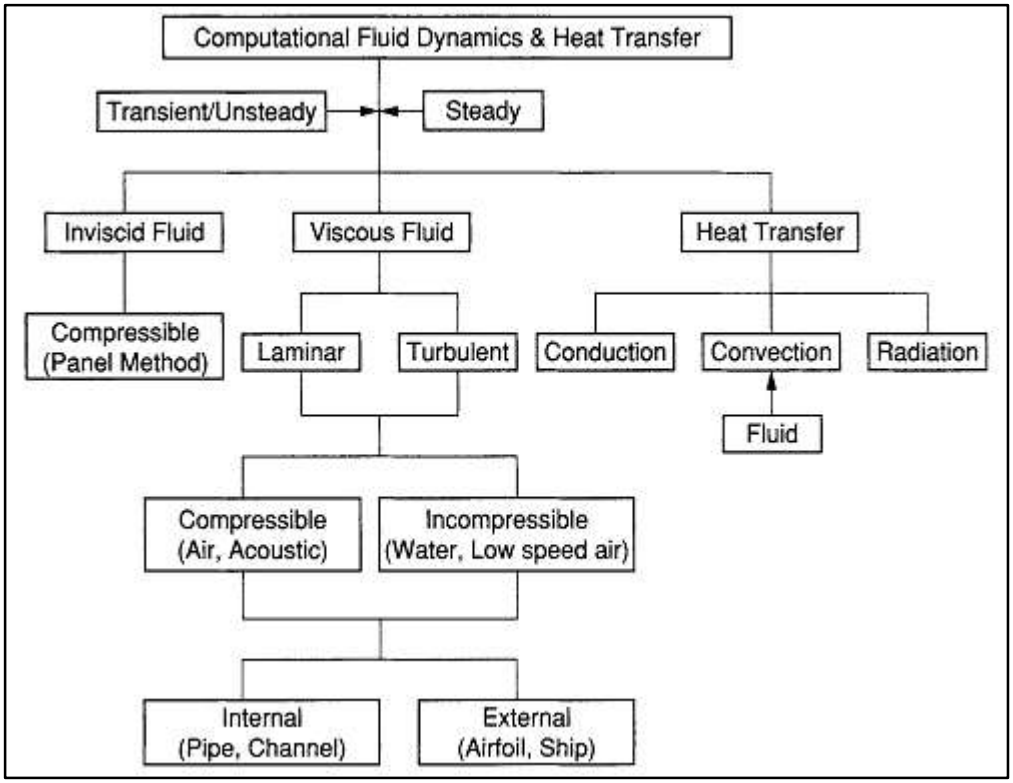

Source: (Tu and others 2007, p. 38)

Air is usually placed on the default settings of many CFD programs likewise at all cases in this research, air is specified as fluid material with its default properties such as density, viscosity, heat capacity, thermal conductivity and etc.

3.2.1.4 Boundary conditions

All CFD problems can be solved dependent to initial and boundary conditions. Initial conditions includes the primitive variables (P, T, u, v, w, k, eps…) and they specify how to start the numerical algorithm.

All CFD algorithms are programmed based on both initial and boundary conditions. The BCs (boundary conditions) should be defined clearly, understood correctly and the BCs of the computational domain is illustrated in Figure 3.12. The inlet and outlet boundary

conditions define the entrance and exit of flow, respectively and can change according to the flow behavior. All cases are solved at hover condition thus there is no velocity income or advance ratio.

Figure 3.12: Boundary condition of the computational domain

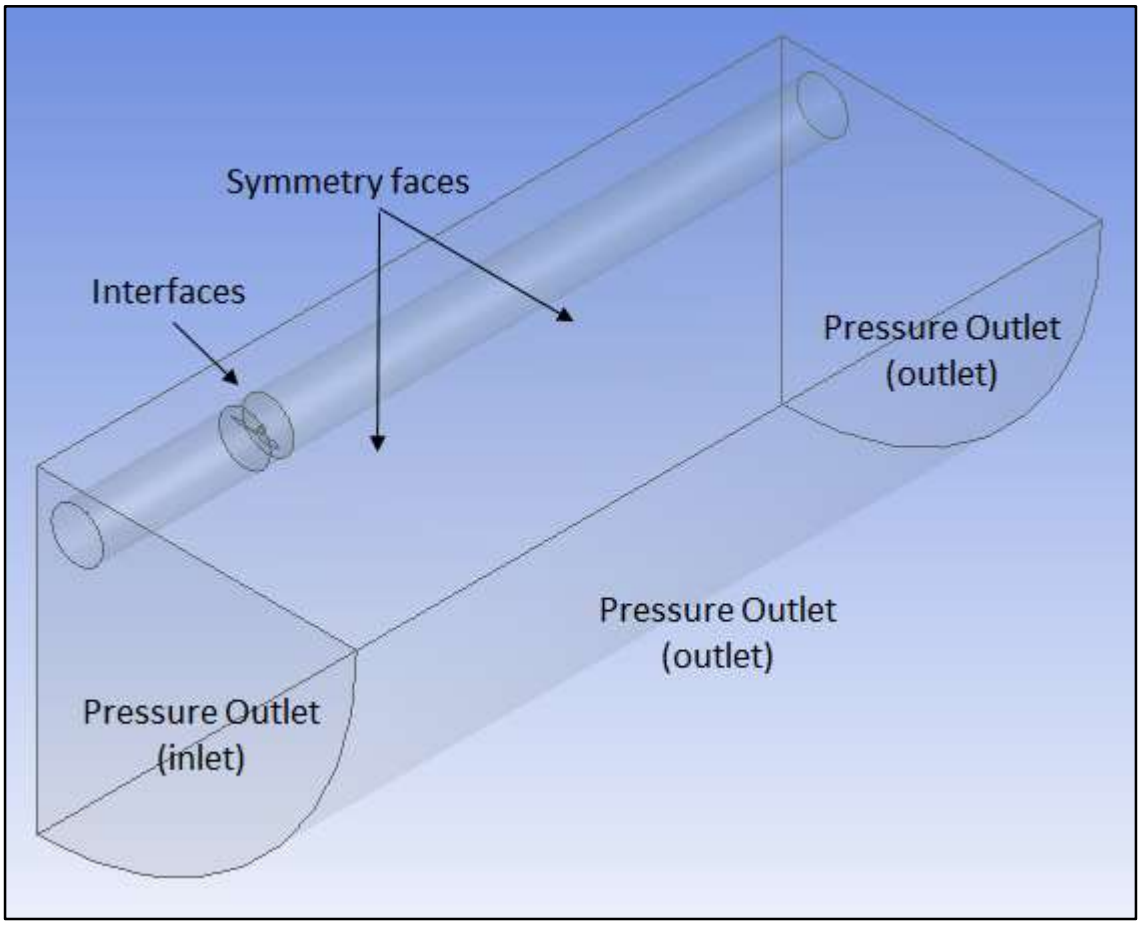

Source: a screenshot from ANSYS Workbench Meshing, captured for this research

The Velocity-Inlet BC is appropriate with inlet velocity 0 m/s. However, the velocity vectors are stuck at inlet area if this BC is used. Thus, the accurate results are not obtained and more detail information is given in the Results section. Otherwise, if the Pressure-Outlet BC is stated at inlet, the accurate results can be obtained. The Pressure-Outlet BC defines only the static/gauge pressure, not interested in any velocity or dynamic variables. Thus, the flow at inlet can move more flexible then an inlet has a Velocity-Inlet BC.

The face at behind of propeller and the cylindrical face are stated as the Pressure-Outlet BC. At hover position of the quadrotor, there is no any advance flow. The rotor just creates a flow and CFD algorithm can calculate velocity vectors by itself.

Figure 3.13: The Inlet BC in ANSYS Fluent

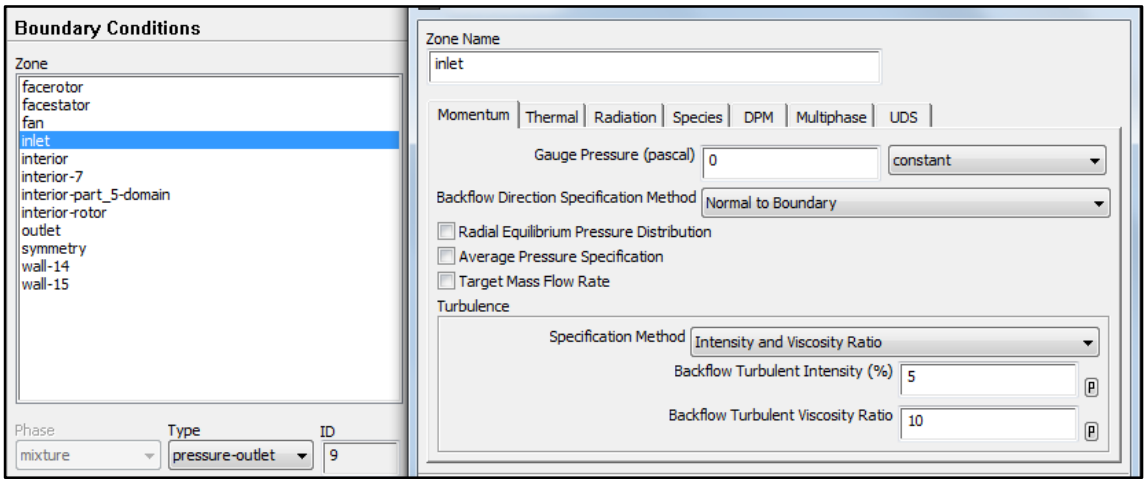

Source: a screenshot from ANSYS Fluent, captured for this research

Symmetry BC make these cases easy to calculate. If the Symmetry BC does not exist, all quadrotor geometry needs to be created. Also, the opposite rotation directions divide the solution domain symmetrically. Therefore, all quadrotor can be divided into 4 quarter domains and only one of them can be calculated. In addition, fewer finite volumes are defined and the CFD problems which have fewer volumes can be run in a shorter time without powerful computers.

If a control volume has more than one domain, the Interface BC has to be placed at coincident faces off different domains. The computational domain is designed as a MRF (Multiple Reference Frame) case. There are 3 coincident faces between rotor and stationary domains and these faces are stated as the Interface BC. Therefore, the flow moves easily from stationary to rotor domain. Moreover, the rotor faces are defined as Wall BC and the rotor is rotating with respect to rotor domain.

3.2.2 CFD Algorithm - Solver

A commercial CFD code or freeware CFD code benefits many fluid problems by presenting the algorithm inside the CFD solver. A CFD solver contains 5 main parts which are initialization, solution control, monitoring solution, CFD calculation and checking for convergence, as illustrated in Figure 3.14. (Tu and others 2007, p. 46)

Figure 3.14: The CFD solver steps

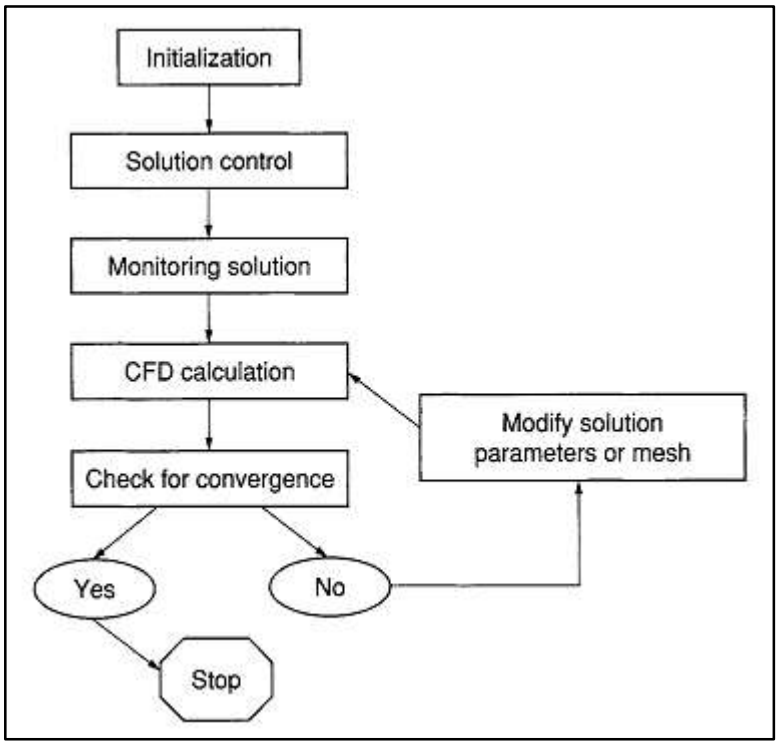

Source: Tu and others 2007, p. 38

3.2.2.1 Initialization and solution control

It is not wrong to say that the 5th step of a CFD analysis is a combination of initialization and solution control prerequisites since the solving of flow problems which include nonlinear and complex physics can be solved successfully with both the right solution algorithm and the logical initialized variables (initial conditions) such as pressure, velocity, density, turbulent energy and etc.

The initial conditions initiate CFD algorithms and they should be specified relevant to flow behavior, thus the residuals can converge in shorter computational time. For instance, the rotor, which has 5000 rpm speed, produces an axial flow that is placed throughout z-axis in the control volume. If the velocity variable in the initial condition is kept at 0 m/s like the default value, as illustrated in Figure 3.15, the solution convergence will take more time. On the other hand, if the velocity variable is set 10 m/s, the convergences will be obtained in a shorter time and the computer will not reach exhausting limits.

Figure 3.15: Initialization and solution control windows

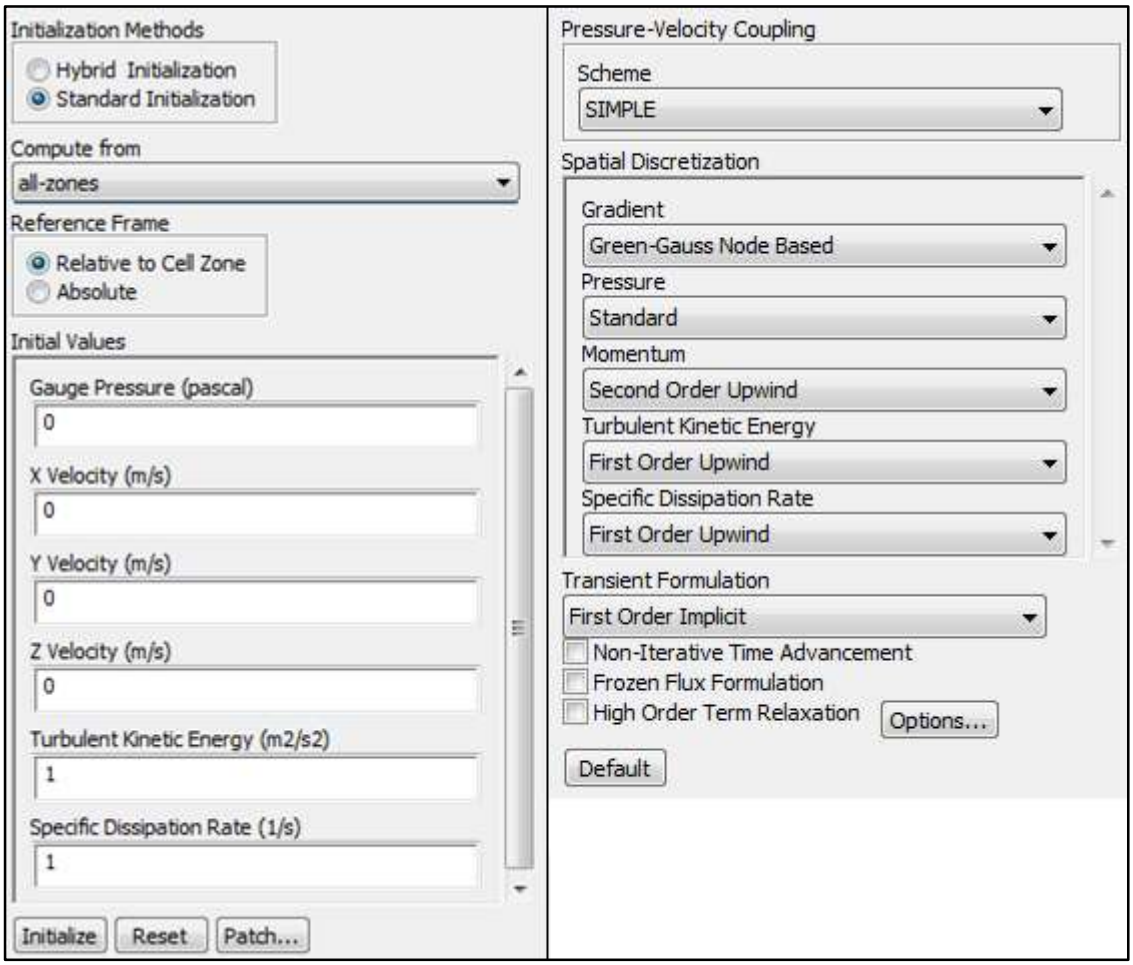

Source: a screenshot from ANSYS Fluent, captured for this research

Most CFD methods are based on the finite-volume method unlike the FEM (Finite Elements Method) which is based on finite-element method. In the finite-volume method, surface fluxes of each cell volume are determined by different interpolation methods such as first order upwind, second order upwind, as illustrated in Figure 3.15. Higher order interpolation methods provide more accurate results. In addition, both smaller and higher order interpolation methods are solved and compared in this study.

Commercial CFD codes may have different interpolation algorithms which are programmed under at least three same fundamental components are gradient, pressure and momentum. Furthermore, these methods are developed under solution algorithms of pressure-velocity coupling such as SIMPLE, SIMPLEC, and PISO. In this research, all

algorithms are run; however the MRF case can be solved under only SIMPLE algorithm. Therefore, all cases are solved with SIMPLE algorithm in this research.

SIMPLE (Semi-Implicit Method for Pressure-Linked Equations) was first proposed by Patankar and Spalding in 1972. SIMPLE actually solves for a relative quantity called pressure correction. The Algorithm guesses an initial flow field and pressure distribution in the computational domain. Then, it maintains to solve the momentum equations iteratively. The pressure field is assumed to be known from the previous iteration. Momentum equations are solved for the velocities. Newly obtained velocities don't satisfy the continuity equation since the pressure field is only guessed. Corrections to velocities and pressure are proposed to satisfy the discrete continuity equation. (Ambatipudi 2011, p. 2)

$$u = u^* + u'$$

$$v = v^* + v'$$

$$p = p^* + p'$$

where u^*, v^*, w^* and p^* are the guess values of velocities in x, y and z directions and pressure, respectively. u', v', w' and p' are the correction values. The SIMPLE algorithm also requires the corrected velocities and pressure to satisfy the momentum equations leading to the corrected momentum equations. (Ambatipudi 2011, p. 2)

Figure 3.16: A structured grid for U-momentum equation

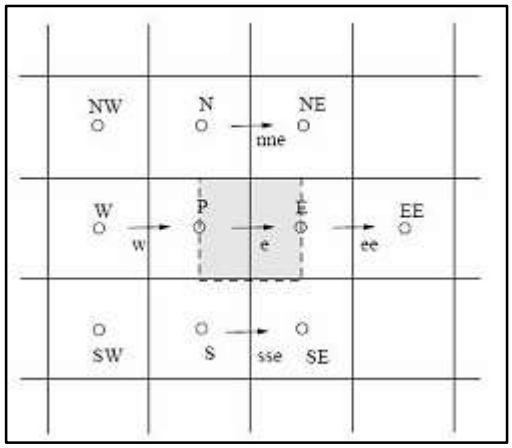

Source: (Ambatipudi 2011, p. 2)

Figure 3.16 shows a structured two-dimensional grid for u-momentum equation. In addition, P indicates the present cell, and the others represents the compass directions. After solved discretized momentum equation to compute the intermediate velocity field, the algorithm computes the uncorrected mass fluxes at faces. It solves the pressure correction equation to produce cell values of the pressure correction and updates the pressure field with the following equation. (Patankar and Spalding 1972, p. 1793-1800)

$$p^{k+1} = p^k + urfx\, p'$$

where urf is the under-relaxation factor for pressure. The under-relaxation factors are explained in section 4.2.1 in more detail. After updates of pressure corrections, it corrects also face mass fluxes with the following equations. (Patankar and Spalding 1972, p. 1793-1800)

$$\dot{m}_f{}^{k+1} = \dot{m}_f{}^{*} + \dot{m}_f{}'$$

The algorithm finally corrects the cell velocities.

$$\vec{u}^{k+1} = \vec{u}^{*} - \frac{Vol\ x\ \nabla p'}{\vec{a}^{v}{}_{p}}$$

where $\nabla p'$ is the gradient of the pressure corrections, $\vec{a}^{v}{}_{p}$ is the vector of central coefficients for the discretized linear system representing the velocity equation and Vol is the volume cell. (Patankar and Spalding 1972, p. 1793-1800)

3.2.2.2 Monitoring convergence

Each calculation steps in a CFD algorithm can be followed by controlling of convergence. Solution algorithms are developed iteratively. That means the continuity equation, the momentum equations and other necessary equations (like turbulent kinetic energy or dissipation equations) are solved repetitively and the magnitudes of differences are expressed by residuals, as illustrated in Figure 3.17.

Figure 3.17: Residuals on a steady flow

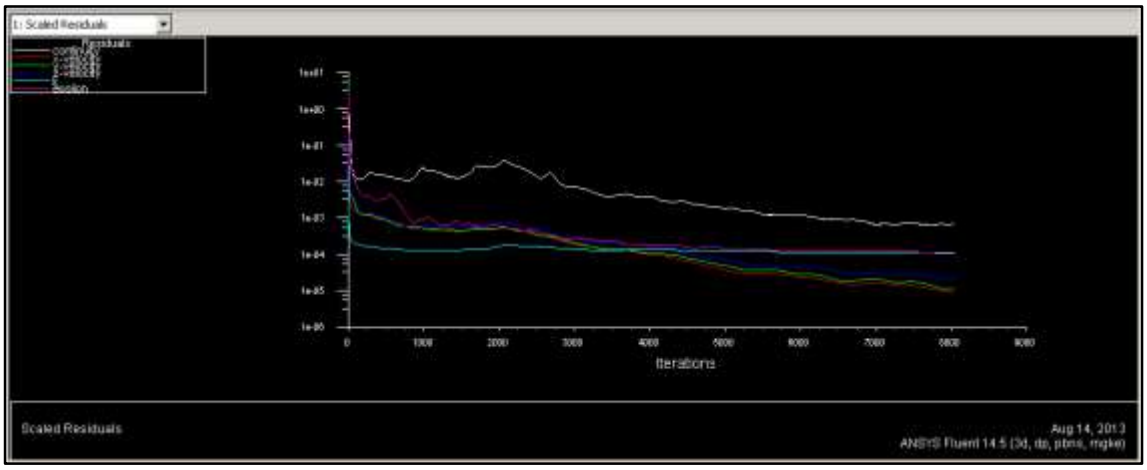

Source: a screenshot from ANSYS Fluent, captured for this research

If residuals fall down, solution will be converged and the user keeps the run until residuals reach the convergence tolerance. A converged solution can be obtained by selecting carefully of the control settings, more quality mesh. Otherwise, the progress can be diverged, residuals rise up and a diverged solution gives wrong information.

Moreover, lift, drag and momentum coefficients can be monitored and the convergences of these variables can be followed easily. For instance, in this research, the lift and drag coefficients of propeller are monitored for each run, as illustrated in Figure 3.18 and Figure 3.19, respectively.

Figure 3.18: Lift coefficient on a steady flow

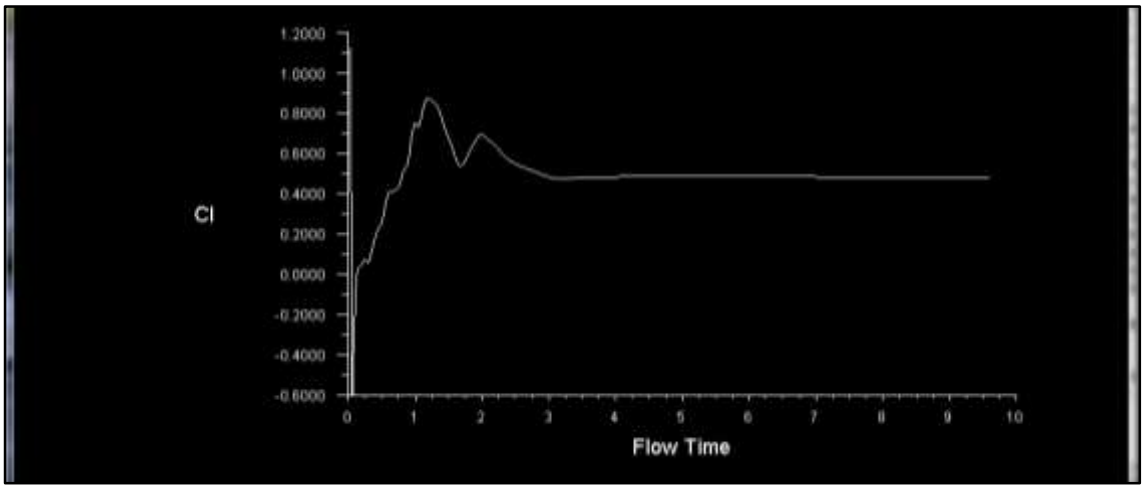

Source: a screenshot from ANSYS Fluent, captured for this research

Figure 3.19: Drag Coefficient on a Steady Flow

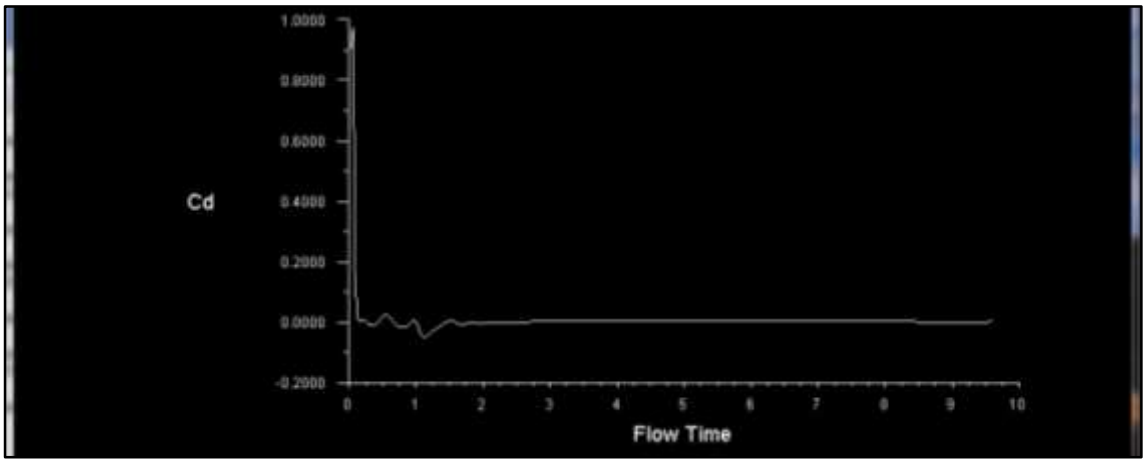

Source: a screenshot from ANSYS Fluent, captured for this research

3.2.3 Reports and Visualization - Post-Process

Analysis of solutions of CFD runs is simplified with powerful post-process tools. Each commercial codes have their own post-process tool such as CFD-Post from ANSYS and also standalone post-process programs are developed for both CFD and FEM analyses such as Ensight and Tecplot.

Post-process tools provide the reporting of any variables such as forces, pressure, and density. Not only on boundaries but also from any place of the computational domain, results can be obtained by cut-planes with vector plots, contour plots, streamlines, surface plots, and also animations. In this research, results are obtained mostly from CFD-Post, rarely from Ensight. An example from CFD-Post is illustrated in Figure 3.20.

Figure 3.20: Pressure contour and velocity vectors example on an axial cut-plane

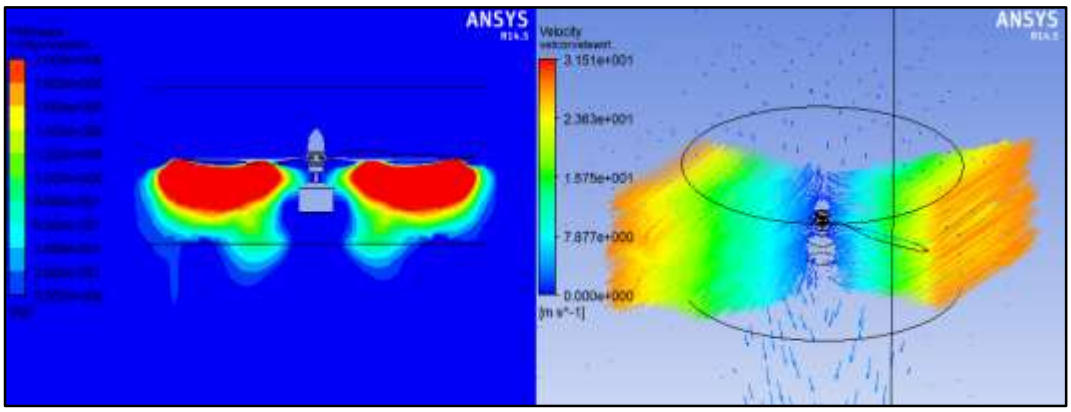

Source: a screenshot from ANSYS CFD-Post, captured for this research

3.3 RUNS

In this study, over 20 cases of both long and short computational domains are run and solutions are compared. Each case has at least one different option such as viscous type or solution control options.

Firstly, the long computational domain is explained with different settings. Secondly, the short domain is explained with different settings, too. The short domain has more number of iteration than the long domain. Thirdly, these cases are compared with a half domain case. Lastly, the quadrotor itself with quarter cylinder geometry is solved symmetrically. All solutions are explained in the Results section.

3.3.1 The Long Computational Domain

The length of the long control volume is 15 m with 5 m entrance long and 10 m outlet long, as illustrated in Figure 3.21.

Figure 3.21: The long computational domain

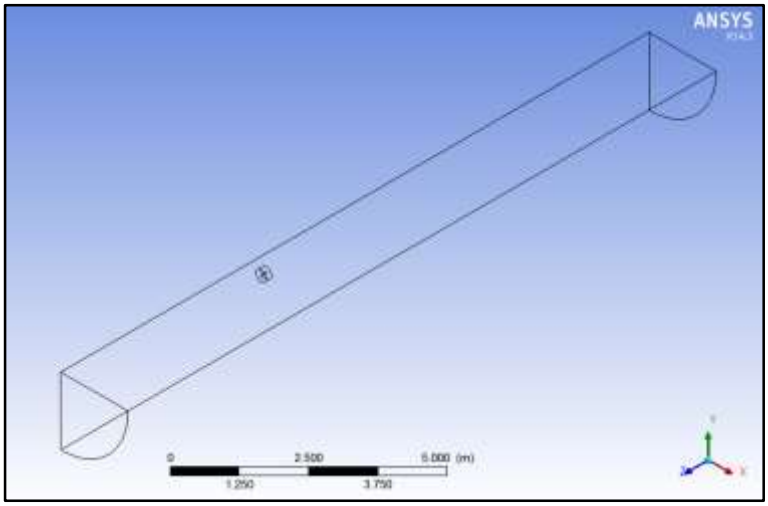

Source: a screenshot from ANSYS Design Modeler, captured for this research

Furthermore, there are five cases for the long control volume and all of them are listed in Table 3.1 with their all mesh specifications and solution control settings. In this table, the case numbers are important since the case numbers of the next tables follow each other. Therefore, this table provides to be understood all compared settings and their results easily.

Table 3.1: Long domain cases with all settings

Case	1	2	3	4	5
Domain Length (m)	15	15	15	15	15
cell number	5505477	5505477	5505477	5429941	5429941
Mesh Quality					
Min Orth. Quality	0,038844	0,038844	0,038844	0,04723	0,04723
Max Aspect Ratio	76,2074	76,2074	76,2074	164,026	164,026
Skewness	0,9721176	0,9721176	0,9721176	0,9753663	0,9753663
Turb. Model	k-w SST	k-w SST	k-w SST	k-w SST	k-w SST
Near-Wall Treatment	Standard	Standard	Standard	Standard	Standard
Time	Transient	Transient	Steady	Transient	Transient
Rotor Rot. Vel. (rpm)	2006	4997	4997	5147	5147
Boundary Conditions					
Inlet	Vel. Inlet	Vel. Inlet	Vel. Inlet	Pres. Out.	Pres. Out.
Vel (m/s) | Pres (Pa)	0	10	10	0	0
Turb. Intensity	5	5	5	5	5
Outlet	Pres. Out.	Pres. Out.	Pres. Out.	Pres. Out.	Pres. Out.
Vel (m/s) | Pres (Pa)	0	0	0	0	0
Turb. Intensity	5	5	5	5	5
Fan	Wall	Wall	Wall	Wall	Wall
Wall Type	Stationary	Moving (0 m/s)	Moving (0 m/s)	Moving (0 m/s)	Moving (0 m/s)
Reference Values					
Area (m2)	1	0,05	0,05	0,05	0,05
Length (m)	1	1	1	1	1
Velocity (m/s)	1	10,323	10,323	10	10
Pres.-Vel. Coupling	**SIMPLE**	**SIMPLE**	**SIMPLE**	**SIMPLE**	**SIMPLE**
Spatial Discretization					
Gradient	Gauss Cell	Gauss Node	Gauss Cell	Gauss Cell	Gauss Node
Pressure	Standard	Standard	Standard	Standard	Standard
Momentum	First Order	First Order	First Order	Second Order	Second Order
Turb. Kinetic En.	First Order	First Order	First Order	First Order	First Order
Specific Diss. Rate	First Order	First Order	First Order	First Order	First Order
Transient Formulation	First Order	First Order		First Order	First Order
Relaxation Factor	0,75	0,75	0,75	0,75	0,75
Calculation					
Time Step Size (s)	0,03	0,0012		0,012	0,012
Max Iter/Time Step	20	20		20	20
Run Time St./Time (s)	321 / 9,63	140 / 0,170		170 / 2,04	50 / 0,6
Iteration	6420	2823	2473	3400	1000
Solution Fan Force (N)	**0,29489663**	**-0,30152845**	**-0,39070282**	**1,9474438**	**2,3393503**

Source: formed by Excel with ANSYS Fluent results

3.3.2 The Short Computational Domain

The length of the short computational domain is 4 m with 1 m entry length and 3 m outlet length, as illustrated in Figure 3.22. Moreover, there are fifteen cases for the short control volume and all of them are listed in Table 3.3 and Table 3.4 with their solution control settings. In these tables, the case numbers resume from the previous table.

Figure 3.22: The short computational domain

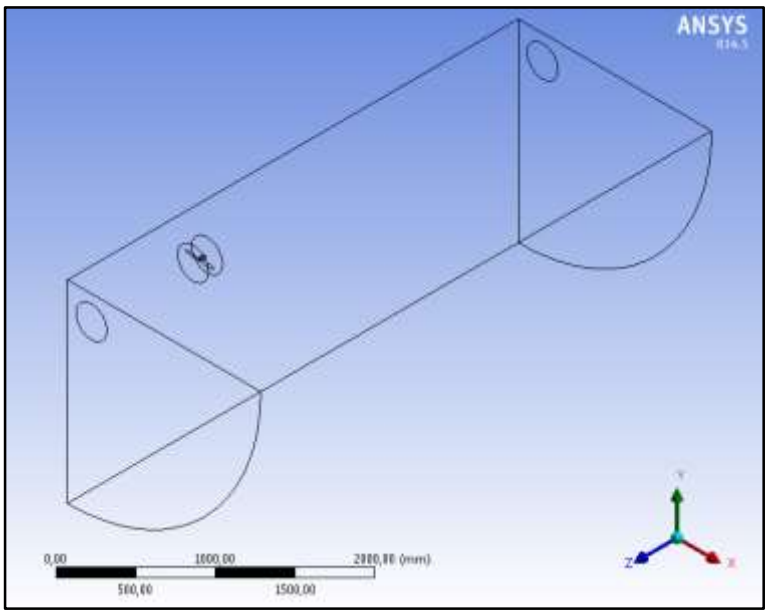

Source: a screenshot from ANSYS Design Modeler, captured for this research

Moreover, in the row of wall type of these tables, there are 2 different arguments; moving (0 m/s) and stationary. Actually, these arguments mention the same meaning. Moving with 0 m/s remains the rotor stationary related to the mesh motion, not the absolute frame.

Furthermore, in mesh quality part, there are 3 remarkable specifications which are min orthogonal quality, max aspect ratio and skewness. Aspect ratio is the ratio of the longest edge length to the shortest edge length.

Figure 3.23: Aspect ratio

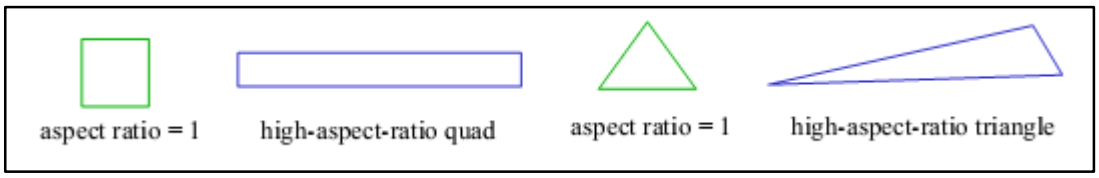

Source: http://www.bakker.org/dartmouth06/engs150/07-mesh.pdf

Skewness is the ratio of the difference between optimal cell size and current cell size to optimal cell size. Range of skewness changes between 0 (best) and 1 (worst).

Figure 3.24: Skewness

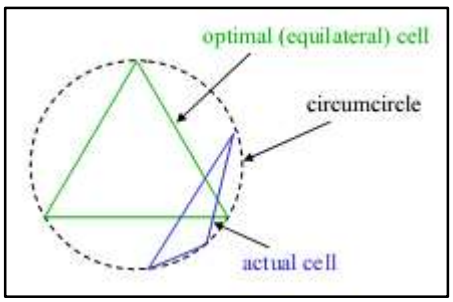

Source: http://www.bakker.org/dartmouth06/engs150/07-mesh.pdf

The orthogonal quality for cells is computed using the face normal vector, the vector from the cell centroid to the centroid of each of the adjacent cells, and the vector from the cell centroid to each of the faces.

Figure 3.25: Orthogonal Quality

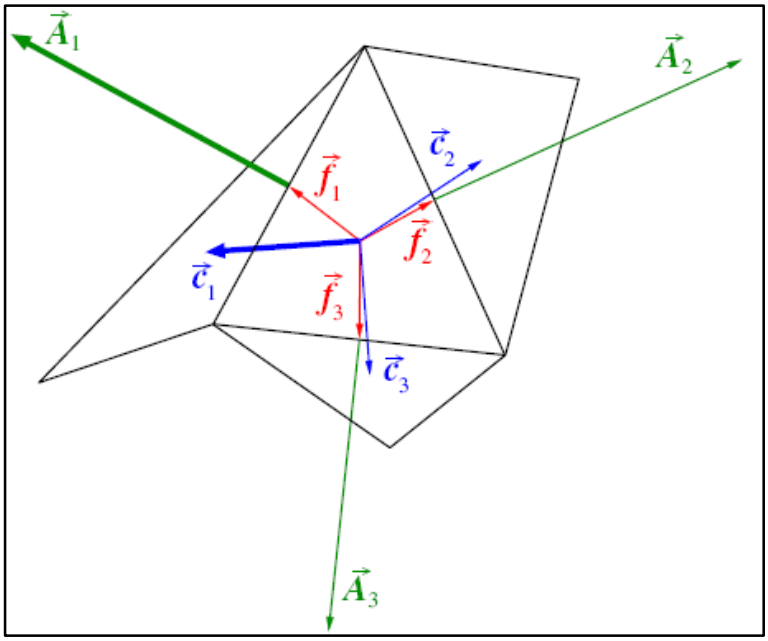

Source:https://www.sharcnet.ca/Software/Fluent14/help/wb_msh/msh_orthogonal_quality.html

Table 3.2: Short domain cases with all settings

Case	6	7	8	9	10
Domain Length (m)	4	4	4	4	4
cell number	5865228	5865228	5865228	5865228	5865228
Mesh Quality					
Min Orth. Quality	0,0425959	0,0425959	0,0425959	0,0425959	0,0425959
Max Aspect Ratio	90,16959	90,16959	90,16959	90,16959	90,16959
Skewness	0,9643137	0,9643137	0,9643137	0,9643137	0,9643137
Turb. Model	k-e RNG	k-e RNG	k-e RNG	k-e RNG	laminar
Near-Wall Treatment	Standard	Enhanced Wall	Standard	Standard	
Time	Steady	Steady	Steady	Steady	Steady
Rotor Rot. Vel. (rpm)	5000	5000	5000	5000	5000
Boundary Conditions					
Inlet	Pres. Out.	Pres. Out.	Pres. Out.	Pres. Out.	Pres. Out.
Vel (m/s) | Pres (Pa)	0	0	0	0	0
Turb. Intensity	5	5	5	5	
Outlet	Pres. Out.	Pres. Out.	Pres. Out.	Pres. Out.	Pres. Out.
Vel (m/s) | Pres (Pa)	0	0	0	0	0
Turb. Intensity	5	5	5	5	
Fan	Wall	Wall	Wall	Wall	Wall
Wall Type	Moving (0 m/s)	Moving (0 m/s)	Stationary	Stationary	Stationary
Reference Values					
Area (m2)	0,05	0,05	0,05	0,05	0,05
Length (m)	1	1	1	1	0,025
Velocity (m/s)	10	10	10	10	10
Pres.-Vel. Coupling	**SIMPLE**	**SIMPLE**	**SIMPLE**	**SIMPLE**	**SIMPLE**
Spatial Discretization					
Gradient	Gauss Cell	Gauss Cell	Least Sq. Cell	Least Sq. Cell	Least Sq. Cell
Pressure	Standard	Standard	Standard	Standard	Standard
Momentum	Second Order	Second Order	Second Order	Second Order	Second Order
Turb. Kinetic En.	Second Order	Second Order	Second Order	Second Order	
Specific Diss. Rate	Second Order	Second Order	Second Order	Second Order	
Relaxation Factor	0,25	0,25	0,25	0,25	0,25
Calculation					
Iteration	8000	5000	6500	3500	7000
Solution Fan Force (N)	**2,0379755**	**2,0253144**	**2,0531143**	**1,9933292**	**2,1197711**

Source: formed by Excel with ANSYS Fluent results

Table 3.3: Short domain cases with all settings (continues from the previous table)

Case	11	12	13	14	15
Domain Length (m)	4	4	4	4	4
cell number	5865228	5865228	5865228	5865228	5865228
Mesh Quality					
Min Orth. Quality	0,0425959	0,0425959	0,0425959	0,0425959	0,0425959
Max Aspect Ratio	90,16959	90,16959	90,16959	90,16959	90,16959
Skewness	0,9643137	0,9643137	0,9643137	0,9643137	0,9643137
Turb. Model	Inviscid	k-e Low-Re	k-e RNG	k-e RNG	k-e RNG
Near-Wall Treatment			Standard	Standard	Enhanced Wall
Time	Transient	Steady	Steady	Steady	Steady
Rotor Rot. Vel. (rpm)	5000	5000	5000	5000	5000
Boundary Conditions					
Inlet	Pres. Out.	Pres. Out.	Pres. Out.	Vel. Inlet	Pres. Out.
Vel (m/s) | Pres (Pa)	0	0	0	10	0
Turb. Intensity		5	0,1	0,1	0,1
Outlet	Pres. Out.	Pres. Out.	Pres. Out.	Pres. Out.	Pres. Out.
Vel (m/s) | Pres (Pa)	0	0	0	0	0
Turb. Intensity		5	5	0,1	0,1
Fan	Wall	Wall	Wall	Wall	Intake-Fan
Wall Type	Stationary	Stationary	Stationary	Stationary	
Pressure Jump (Pa)					200
Reference Values					
Area (m2)	0,05	0,05	0,05	0,05	0,05
Length (m)	1	1	0,25	0,25	0,25
Velocity (m/s)	10	10	10	10	10
Pres.-Vel. Coupling	**Coupled**	**SIMPLE**	**SIMPLE**	**SIMPLE**	**SIMPLE**
Spatial Discretization					
Gradient	Least Sq. Cell	Least Sq. Cell	Least Sq. Cell	Least Sq. Cell	Least Sq. Cell
Pressure	Standard	Standard	Standard	Standard	Standard
Momentum	Second Order	Second Order	Second Order	Second Order	Second Order
Turb. Kinetic En.		Second Order	Second Order	Second Order	Second Order
Specific Diss. Rate		Second Order	Second Order	Second Order	Second Order
Transient Formulation	First Order				
Relaxation Factor	0,75	0,25	0,25	0,25	0,25
Calculation					
Time Step Size (s)	0,012				
Max Iter/Time Step	20				
Run Time St./Time (s)	225 / 2,7				
Iteration	4500	6000	5000	5000	7000
Solution Fan Force (N)	**1,9536503**	**1,9023772**	**2,0024594**	**-0,25055346**	**-2.43051**

Source: formed by Excel with ANSYS Fluent results

Table 3.4: Short domain cases with all settings (continues from the previous table)

Case	16	17	18	19	20
Domain Length (m)	4	4	4	4	4
cell number	5603771	5603771	5603771	5603771	4968762
Mesh Quality					
Min Orth. Quality	0,0502316	0,0502316	0,0502316	0,0502316	0,0592324
Max Aspect Ratio	60,5224	60,5224	60,5224	60,5224	58,462
Skewness					0,9932169
Turb. Model	k-w SST	k-w SST	k-w SST	k-w SST	k-e RNG
Near-Wall Treatment					Standard
Time	Transient	Transient	Transient	Transient	Steady
Rotor Rot. Vel. (rpm)	5000	5000	5000	5000	2000
Boundary Conditions					
Inlet	Pres. Out.	Pres. Out.	Pres. Out.	Pres. Out.	Vel. Inlet
Vel (m/s) | Pres (Pa)	0	0	0	0	0
Turb. Intensity	5	5	5	5	5
Outlet	Pres. Out.	Pres. Out.	Pres. Out.	Pres. Out.	Pres. Out.
Vel (m/s) | Pres (Pa)	0	0	0	0	0
Turb. Intensity	5	5	5	5	5
Fan	Wall	Wall	Wall	Wall	Wall
Wall Type	Moving (0 m/s)	Moving (0 m/s)	Moving (0 m/s)	Moving (0 m/s)	Moving (0 m/s)
Reference Values					
Area (m2)	0,05	0,05	0,05	0,05	0,05
Length (m)	1	1	1	1	1
Velocity (m/s)	26,25	26,25	26,25	26,25	26,25
Pres.-Vel. Coupling	**SIMPLE**	**SIMPLE**	**SIMPLE**	**SIMPLE**	**SIMPLE**
Spatial Discretization					
Gradient	Gauss Node	Gauss Node	Gauss Node	Gauss Node	Gauss Cell
Pressure	Standard	Standard	Standard	Standard	Standard
Momentum	First Order	Second Order	Second Order	Second Order	Second Order
Turb. Kinetic En.	First Order	First Order	First Order	Second Order	Second Order
Specific Diss. Rate	First Order	First Order	First Order	Second Order	Second Order
Transient Formulation	First Order	First Order	First Order	Second Order	
Relaxation Factor	0,75	0,75	0,75	0,75	0,25
Calculation					
Time Step Size (s)	0,012	0,012	0,0012	0,0012	
Max Iter/Time Step	20	20	20	20	
Run Time St./Time (s)	34 / 0,408	285 / 3,42	440 / 0,528	280 / 0,342	
Iteration	667	5700	8800	5681	9000
Solution Fan Force (N)	**2,0328978**	**1,4680311**	**1,899773**	**2,5080612**	**0,32817194**

Source: formed by Excel with ANSYS Fluent results

3.3.3 Benchmarking with Periodic Half Domain for the Propeller Only

This case is set to validate the results of the previous cases. Half propeller (one pal) is modelled into half cylinder computational domain and the dimensions of the control volume is 2 times larger than short computational domain. It means the length of half domain is 8 m long with 2 m entrance long and 6 m outlet long.

This propeller is not a symmetrical geometry since one blade of the propeller follows the other. That means a periodic geometry, thus the results from both short and long domains can be compared with a periodic domain. Moreover, a benchmark case is gained for this research.

Figure 3.26: Periodic half domain geometry

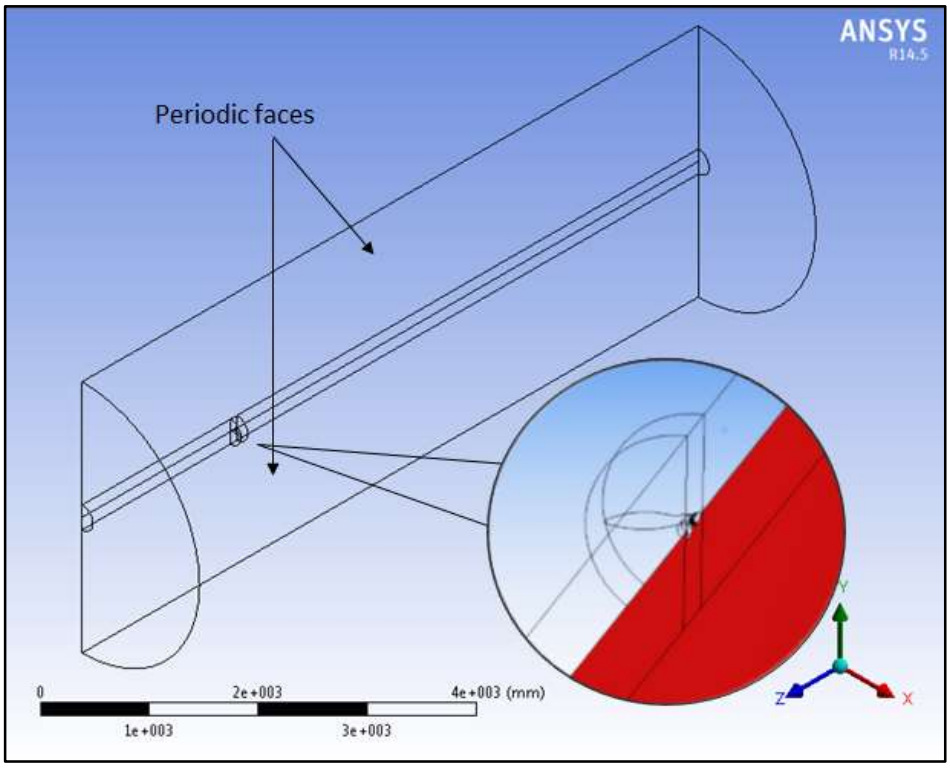

Source: a screenshot from ANSYS Design Modeler, captured for this research

The axial surface is divided into two faces thus the periodic faces can be set. One of them is indicated with red in Figure 3.26. After setting the periodic faces, other conditions can be set like other MRF cases. In addition, all settings with mesh quality and solution control settings are listed in Table 3.5.

Table 3.5: Periodic half domain with all settings

Domain Length (m)	8	**Fan**	Wall
cell number	4150244	Wall Type	Stationary
Mesh Quality		**Reference Values**	
Min Orth. Quality	0,0724717	Area (m2)	0,05
Max Aspect Ratio	124,55	Length (m)	1
Skewness	0,985522269	Velocity (m/s)	10
Turb. Model	k-e RNG	**Pres.-Vel. Coupling**	**SIMPLE**
Near-Wall Treatment	Standard	**Spatial Discretization**	
Time	Steady	Gradient	Least Sq. Cell
Rotor Rot. Vel. (rpm)	5000	Pressure	Standard
Boundary Conditions		Momentum	Second Order
Inlet	Pres. Out.	Turb. Kinetic En.	Second Order
Vel (m/s) | Pres (Pa)	0	Specific Diss. Rate	Second Order
Turb. Intensity	5	Relaxation Factor	0,25
Outlet	Pres. Out.	**Calculation**	
Vel (m/s) | Pres (Pa)	0	Iteration	10000
Turb. Intensity	5	**Solution Fan Force (N)**	**1,0266519**

Source: formed by Excel with ANSYS Fluent results

3.3.4 Quadrotor Itself

A quadrotor is designed symmetrically into a quarter cylinder likewise main domains, as illustrated in Figure 3.27. In addition, this domain has same dimensions with short computational domain. All settings are listed in Table 3.6.

Figure 3.27: Quadrotor geometry in symmetric domain

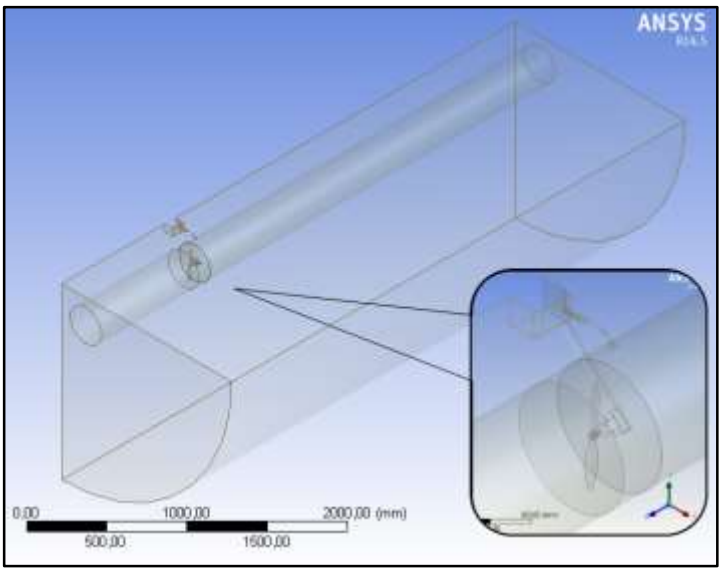

Source: a screenshot from ANSYS Design Modeler, captured for this research

This domain has less cell number than other cases since this domain is solved with inviscid model. That means there is no shear stress in flow. The algorithm calculates only pressure and not any viscous forces. The aim of this case is to check only lift force.

Table 3.6: Quadrotor domain with all settings

Domain Length (m)	4	**Fan**	Wall
cell number	1217870	**Reference Values**	
Mesh Quality		Area (m2)	0,05
Min Orth. Quality	0,0753777	Length (m)	0,12
Max Aspect Ratio	57,7652	Velocity (m/s)	10
Skewness	0,971799347	**Pres.-Vel. Coupling**	**SIMPLE**
Turb. Model	Inviscid	**Spatial Discretization**	
Time	Steady	Gradient	Gauss Node
Rotor Rot. Vel. (rpm)	5000	Pressure	Second Order
Boundary Conditions		Momentum	Second Order
Inlet	Pres. Out.	Relaxation Factor	0,25
Vel (m/s) | Pres (Pa)	0	**Calculation**	
Outlet	Pres. Out.	Iteration	8800
Vel (m/s) | Pres (Pa)	0	**Solution Fan Force (N)**	**2,0903624**

Source: formed by Excel with ANSYS Fluent results

4. RESULTS

In this section, the cases which have right solutions are just explained in detail. The rest of them are summarized shortly.

4.1 THE LONG COMPUTATIONAL DOMAIN

All cases have long computational domain are calculated with k-w SST model. First 3 cases have same grid and velocity inlet BCs. On the other hand, the rest of them have different mesh and also pressure outlet BCs as inlet.

4.1.1 Case 4 and 5

Case 1 is the one of the wrong runs since the velocity inlet BC with 0 m/s compresses the air, not let to treat flexible. Accordingly, the air cannot move at inlet and the run gives the wrong results. Case 1, case 2 and case 3 have the same solution domain with same grid. However, both case 2 and 3 have an advance velocity with 10 m/s since the advance velocity is preferred to understand why the stuck flow occurs.

Case 4 and 5 are solved with k-w SST model in transient time, however they have a different grid and different inlet BC. The pressure outlet BC is set instead of velocity inlet BC. As explained in section 3.2.1.4, pressure outlet states only static pressure, not dynamic pressure. If the pressure outlet is set in both inlet and outlet, the propeller rotation can calculate flow dynamics. Thus, the accurate results can be obtained.

Although the rotor is modelled with wall BC totally, the motor and blades are modelled separately in these two cases. Despite the motor rotation, the motor does not generate any lift, causing some drag. Since all lift forces are generated by blades, they are set wall BC separately from the motor, as illustrated in Figure 4.1.

Furthermore, there is a difference between case 4 and 5. Case 4 is solved with cell based like case 3. However, case 5 is solved node based like case 2. On the other hand, the calculations of both case 4 and 5 do not take much time. The time step size is set with 0.012 s that means the rotor rotates one revolution if the angular velocity is set 5000 rpm.

Case 4 runs with 170 time steps means it takes 2.04 s. Case 5 runs with 50 time steps it takes 0.6 s.

Figure 4.1: Blades are separated from the motor of case 4 and 5

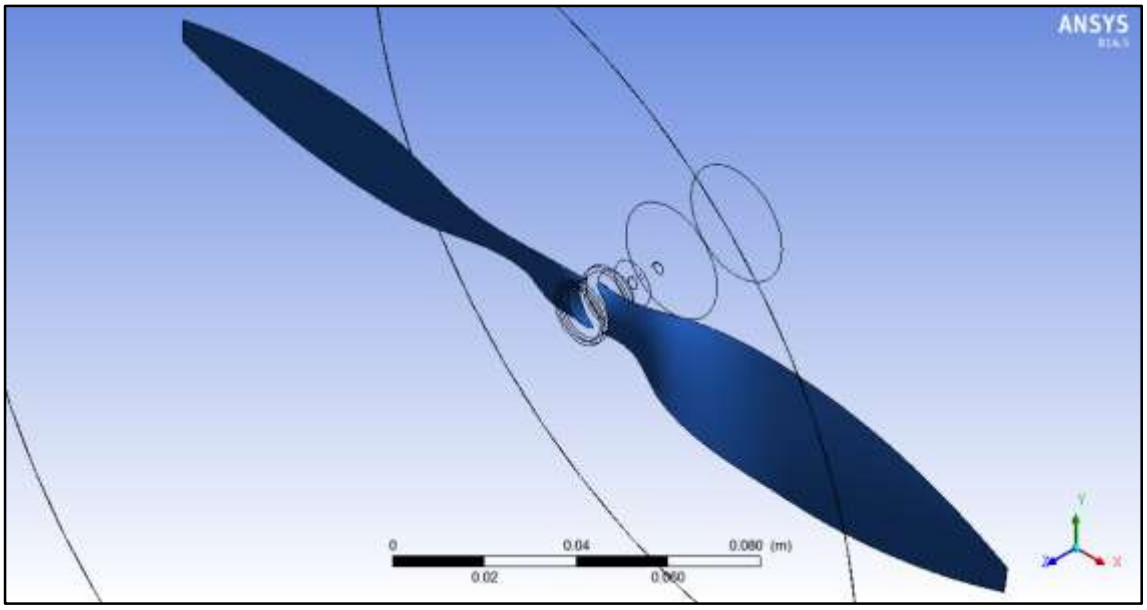

Source: a screenshot from ANSYS CFD-Post, captured for this research

Figure 4.2: Streamlines on case 4 and case 5

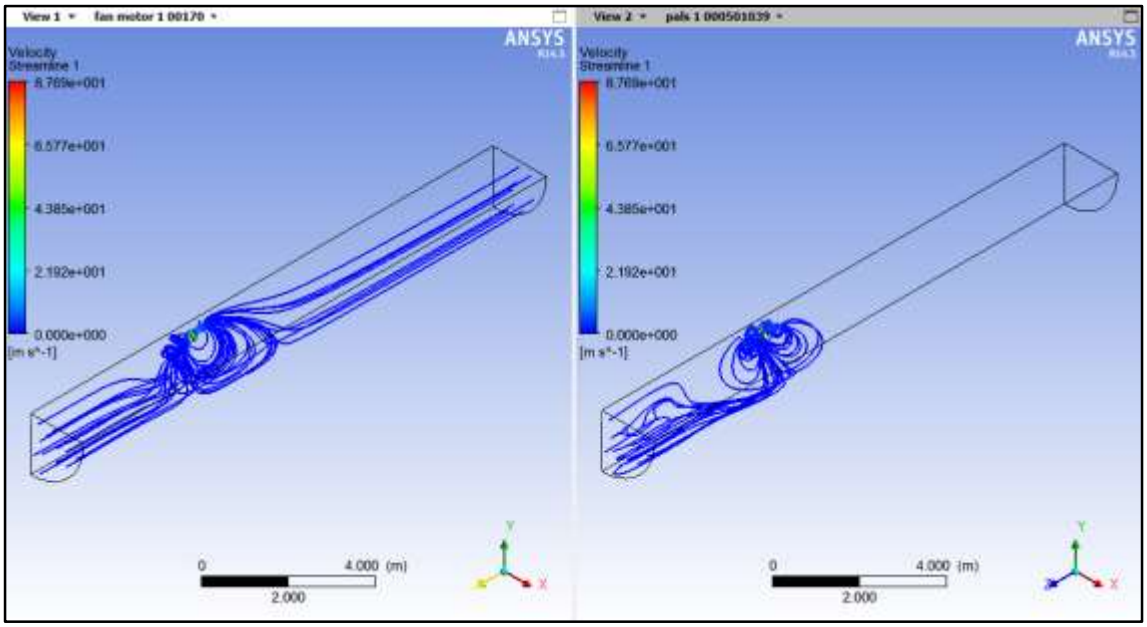

Source: a screenshot from ANSYS CFD-Post, captured for this research

Although the obtained thrust forces of case 4 and 5 are 1.9474438 N and 2.3393503 N, respectively, the streamlines shows the flow does not fully developed in both cases.

However, they also shows that if a case run with more time step or iteration, more accurate results will be obtained. These transient cases should run at least 250 ~ 300 time steps in order to get accurate results. In Figure 4.2, the left image of case 4 have more accurate results than the right image of case 5.

4.2 THE SHORT COMPUTATIONAL DOMAIN

Other 15 cases are solved with short solution domain. The computer capacity used for this thesis can solve a case has up to 6 million mesh with 8 cores. There are two different grid number of the long domain; 5505477 and 5429941, respectively. If a shorter domain is modelled with same grid number, the mesh sizes will get smaller and the mesh quality will increase. All short domain cases are listed in Table 3.2, Table 3.3, and Table 3.4.

Therefore, a short computational domain is modelled in order to get more accurate results. There are three different mesh number of the short domain; 5865228, 5603771 and 4968762, respectively. Cases 6 to 15 are solved with the domain has 5865228 grid number, cases 16 to 19 are solved with the domain has 5603771 grid number and case 20 is solved with the domain has 4968762 grid number.

4.2.1 Cases 6 to 9

Case 6, 7, 8 and 9 are solved with k-eps RNG viscous model in steady time. All of them have the same boundary conditions. The inlet and outlet BCs are the pressure outlet with 0 Pa and also the rotor rotates with 5000 rpm. Both case 6 and 7 uses the gradient computation with gauss-cell based method otherwise both case 8 and 9 uses with least-square-cell based. These four cases are listed in Table 3.2 with all settings.

Gauss cell based gradient evaluation computes the arithmetic average of the values of both the present cell center and the next neighbor's cell center. However, least square method gradient evaluation computes the minimization problem for the system of the non-square coefficient matrix in a least-squares sense. This linear system equation solves the coefficient matrix by using Gram-Schmidt process. (Anderson and Bonhaus 1994, p. 8)

The difference between case 6 and 7 is the wall function. The k-eps viscous models can be calculated with various wall functions. Case 6 is solved with standard wall function

otherwise case 7 is solved with enhanced wall function. Standard wall function can work dependent on y plus (y+) that is the dimensionless wall distance for a wall-bounded flow. On the other hand, enhanced wall function can work independently from y+. However, it affects the epsilon since they work together. Figure 4.3 shows how enhanced wall function can affect the epsilon variable.

Figure 4.3: The residual plots of case 6 and 7

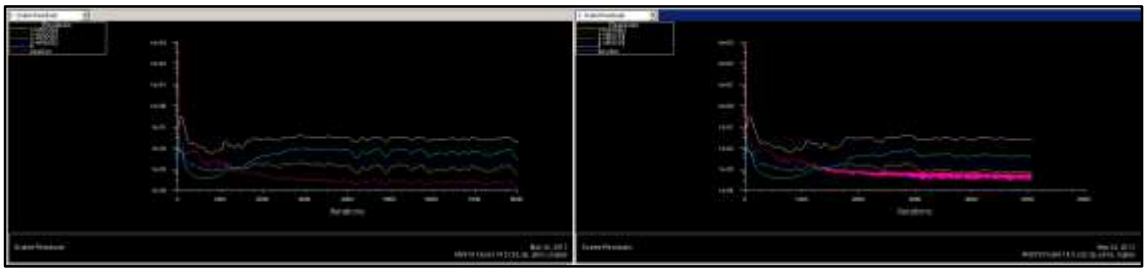

Source: a screenshot from ANSYS Fluent, captured for this research

Although the epsilon variable is affected by a different wall function, the thrust forces of case 6 and 7 are too similar that are 2.0379755 N and 2.0253144 N, respectively. Figure 4.4 shows similar axial velocity contours of case 6 and 7 and supports thrust force results.

Figure 4.4: Axial velocity contours of case 6 and 7

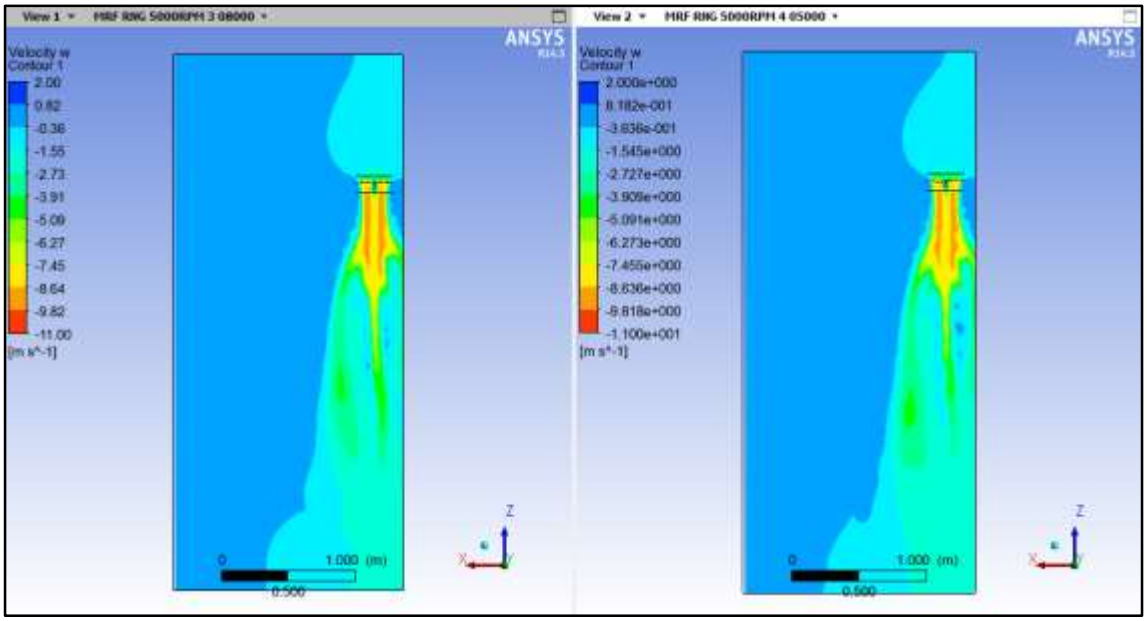

Source: a screenshot from ANSYS CFD-Post, captured for this research

On the other hand, the difference between case 8 and 9 is the under-relaxation factors. Under-relaxation factors affect the solution convergence directly since they check the

update of the computed variable at each iteration. In addition, they take part of the value from previous iteration in order to damp the solution oscillations. Case 9 only has the reduced under-relaxation factors otherwise case 8 has the default under-relaxation factors, as listed in Table 4.1. Figure 4.5 shows more reduced under-relaxation factors provides less oscillated residuals.

Table 4.1: Under-Relaxation factors of case 8 and 9

Under-Relaxation Factors	Case 8	Case 9
Pressure	0,3	0,1
Density	1	0,7
Body Forces	1	0,7
Momentum	0,7	0,5
Turb. Kinetic Energy	0,8	0,5
Specific Dissipation Rate	0,8	0,5
Turb. Viscosity	1	0,7

Source: formed by Excel with ANSYS Fluent settings

Figure 4.5: Residuals of case 8 and 9

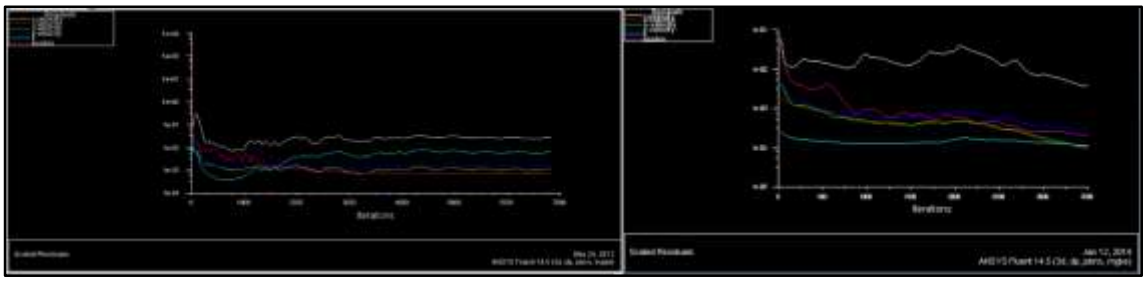

Source: a screenshot from ANSYS Fluent, captured for this research

Figure 4.6 indicates the tangential velocity contours of both case 8 and 9. The contours seems different since case 8 and 9 are run with 6500 and 3500 iterations, respectively. That is also caused by the difference of under-relaxation factor. In conclusion, case 8 and 9 gives the thrust forces with 2.0531143 N and 1.9933292 N, respectively.

Figure 4.6: Tangential velocity contours of case 8 and 9

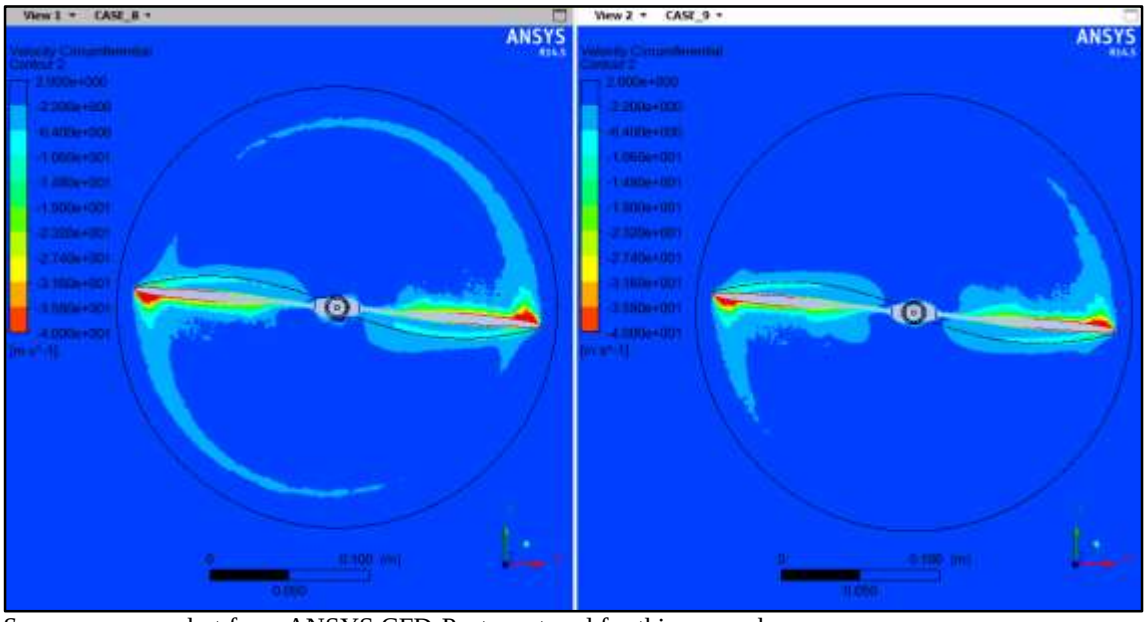

Source: a screenshot from ANSYS CFD-Post, captured for this research

4.2.2 Cases 10 to 13

Cases 10, 11, 12 and 13 are maintain solving with the same least-square cell based gradient evaluation and the same reduced under-relaxation factor like case 9. However, different viscous models are chosen for these cases. Case 10, 11 and 12 is used with laminar, inviscid and k-eps Low-Re models, respectively. Case 13 settings are similar to case 9 but the inlet BC settings include pressure outlet with 0.1 turbulence intensity.

Figure 4.7: Residuals of case 10

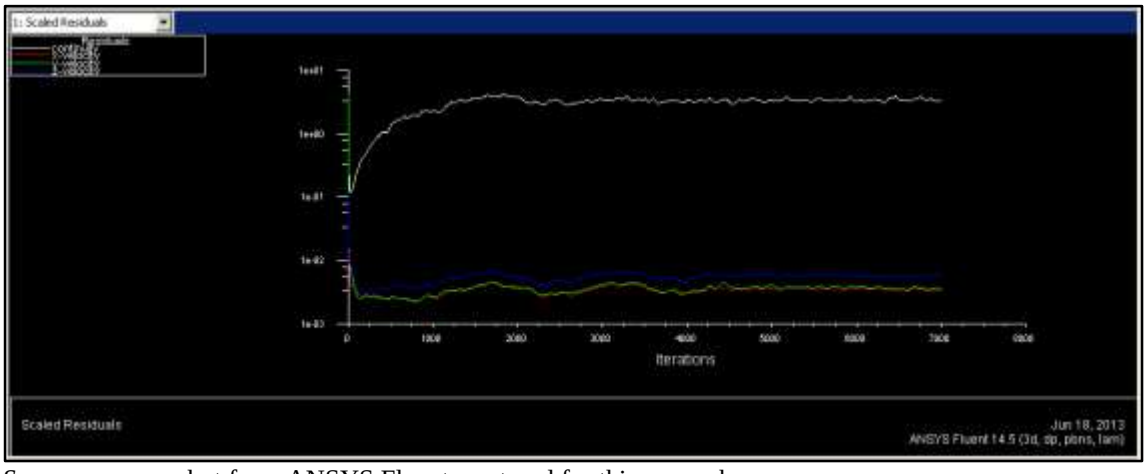

Source: a screenshot from ANSYS Fluent, captured for this research

Figure 4.7 indicates the residuals of case 10 but the continuity equation line is above the zero although the momentum equations lines are below the zero. All residuals must be below the zero to express if a study is true. Despite the wrong residuals, the thrust force is obtained as 2.1197711 N.

The laminar model is also chosen since the max tangential velocity magnitude is 40 m/s in the previous cases approximately. If the Reynolds number is calculated with the following equation to check the flow type,

$$Re = \frac{\rho v D_H}{\mu}$$

where ρ is air density, v is the inlet velocity, $D_H$is the characteristic length and μ is the dynamic viscosity. (Tu and others 2007, p. 90) The Reynolds number is

$$Re = \frac{1.225\ {}^{kg}/_{m^3} * 40\ {}^{m}/_{s} * 0.025\ m}{1.7894e-05\ {}^{kg}/_{ms}} = 68458$$

Reynolds number is smaller than 100000 that means the flow behaves laminar.

Case 11 is solved with inviscid model which does not include any shear stress. The algorithm calculates only momentum, no any viscous forces. The calculation of pressure levels is enough to determine the lift force. However, the viscous forces should be also calculated to get more accurate results.

This case is solved in transient time and gives 1.9536503 N thrust force. Figure 4.8 shows the residuals in transient time. In steady flow, the initial conditions are used once during the run but in unsteady flow, the refreshed initial condition in present time step is produced from the previous time step after the initial conditions are used firstly.

Figure 4.8: Residuals of case 11

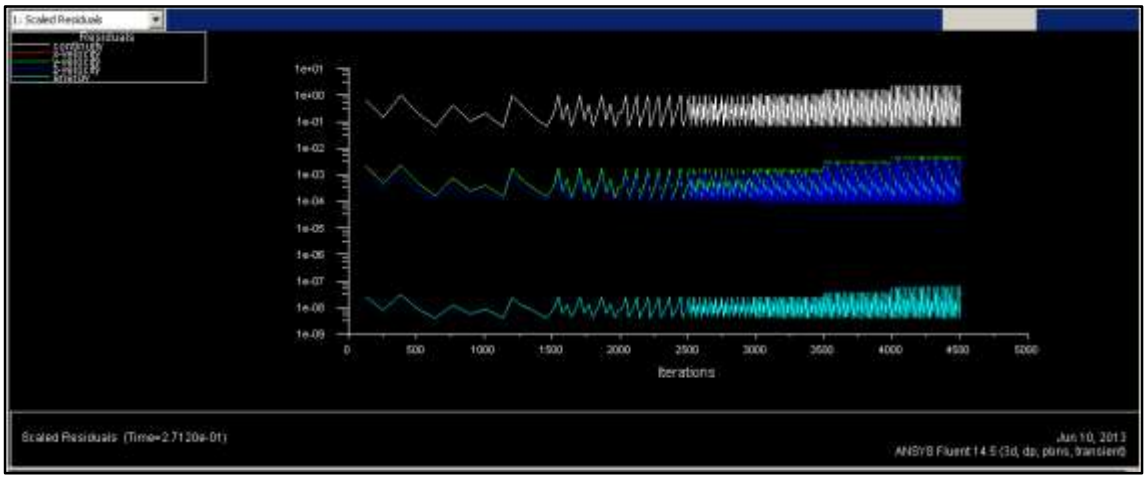

Source: a screenshot from ANSYS Fluent, captured for this research

The low-Re k-eps viscous model is preferred in case 12 since the Reynolds number is 68458.7 is quite small for an open channel flow. In addition, the Mach number is calculated with the following formula;

$$M = \frac{v}{v_{sound}} = \frac{40\ {}^{m}/_{s}}{340\ {}^{m}/_{s}} = 0.11$$

where v is the velocity and v_{sound} is the velocity of sound. Mach number is quietly smaller than 0.8 that means the flow is subsonic. (Anderson 2001, p. 57) The case has low Re or low Mach number can be also solved with low-Re k-eps viscous model. The thrust force of case 12, whose residuals plot is illustrated in Figure 4.9, is 1.9023772 N.

Figure 4.9: Residuals of case 12

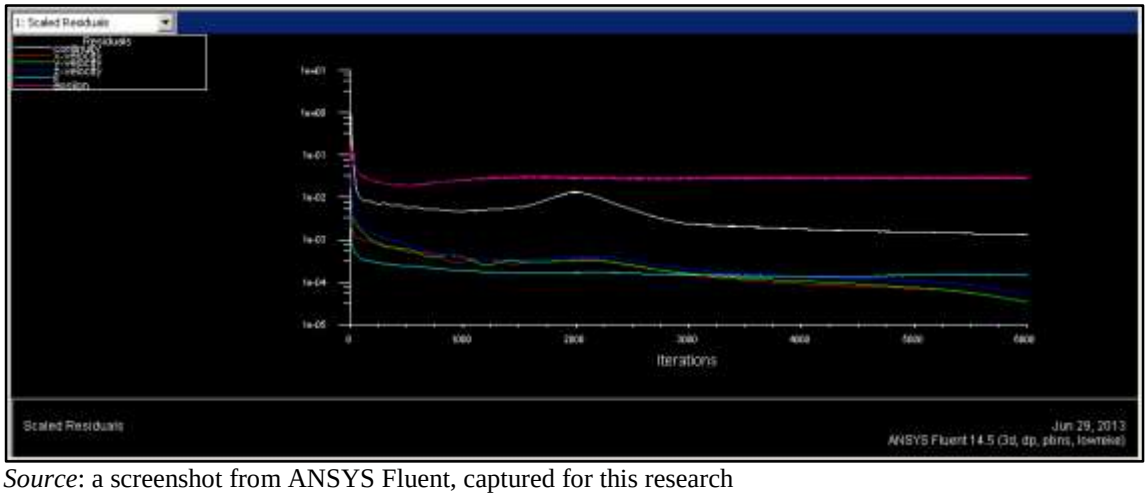

Source: a screenshot from ANSYS Fluent, captured for this research

Case 13 is similar to case 9 but inlet BC settings include pressure outlet with 0.1 turbulence intensity since the turbulence intensity is set as nearly 0.1 in the subsonic wind tunnel experiments of Brandt and Selig (2011). The objective of this case is the preparation a benchmark with this study. However, the results maintain similar to the previous cases instead of the wind tunnel experiments. The thrust force is 2.0024594 N. Figure 4.10 and Figure 4.11 indicate the residuals and streamlines, respectively.

Figure 4.10: Residuals of case 13

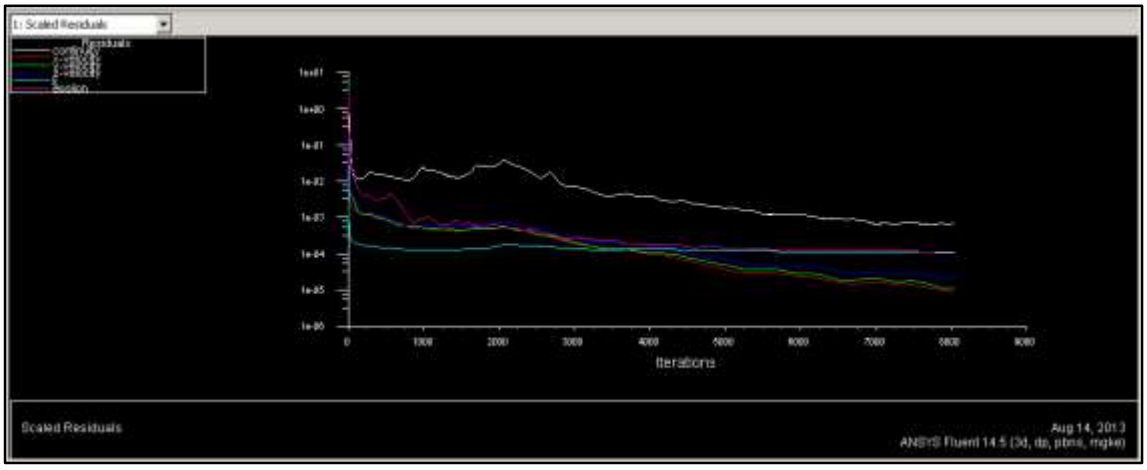

Source: a screenshot from ANSYS Fluent, captured for this research

Figure 4.11: Streamlines of case 13

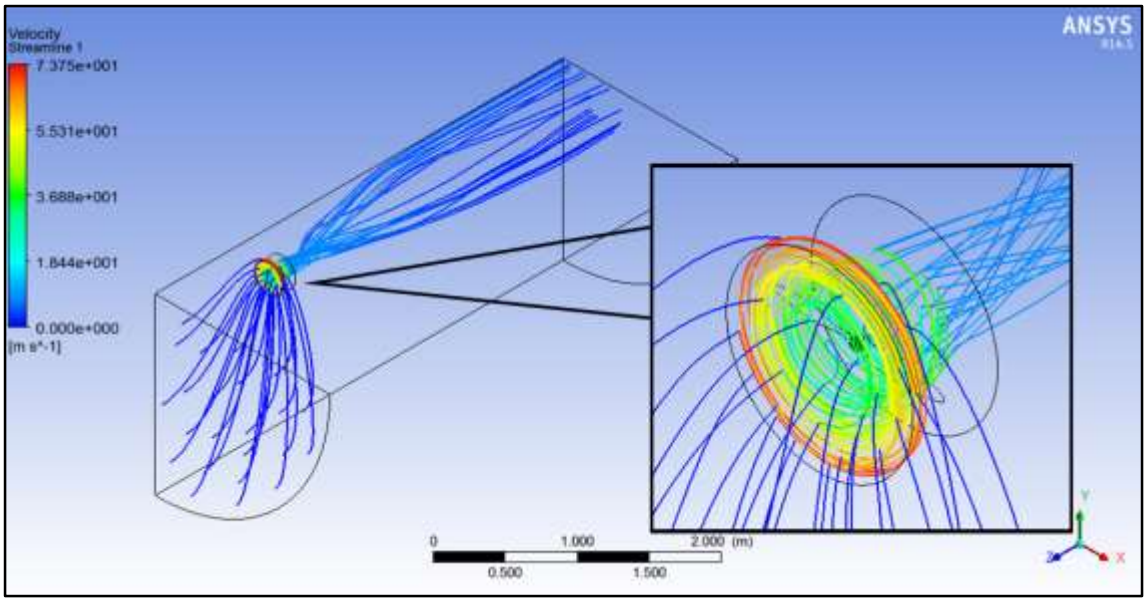

Source: a screenshot from ANSYS CFD-Post, captured for this research

4.2.3 Cases 16 to 19

Cases 14 and 15 have the wrong results in this study. Case 14 has the velocity inlet BC with the same advance velocity of cases 2 and 3. Case 15 has totally different propeller BC which is intake-fan. Intake-fan BC works with pressure drop method. In this case, pressure drop value is set 200 Pa as a constant value. This value is obtained the results from the previous cases by probing the relative pressure at both below and above propeller surface. Moreover, the intake-fan BC is chosen for non-complex geometry, not for the complex geometry like propeller.

Cases 16, 17, 18 and 19 are solved with k-w model in transient time. Cases 16 and 17 have the time step size with 0.012 s, the propeller rotates just one revolution in each time step. On the other hand, cases 18 and 19 have time step size with 0.0012 s, the propeller rotates 10 revolutions in each time step.

There is one difference between case 16 and 17. The momentum equations are set as second order in case 17 and case 16 keeps it as first order. However, case 16 works with 34 time steps are equals to 667 iterations. As mentioned before in 4.1.1, a case should be run with more time steps to get accurate results. Despite less time steps, case 16 gives the thrust force with 2.0328978 N. The residuals of case 16 and 17 is illustrated in Figure 4.12.

Figure 4.12: Residuals of case 16 and 17

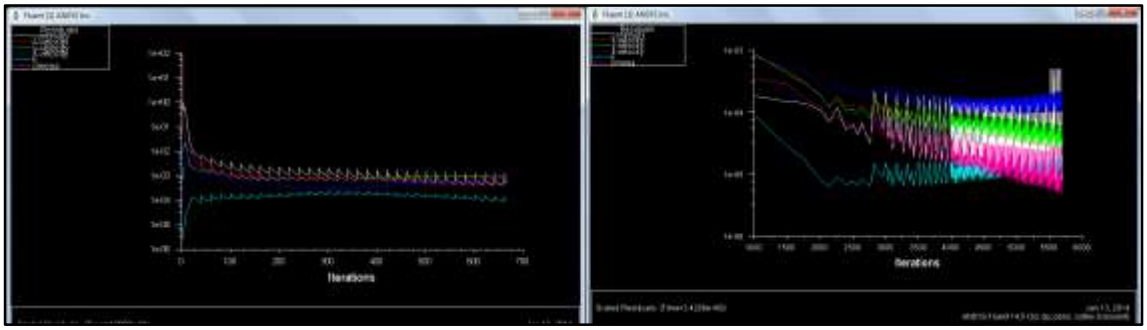

Source: a screenshot from ANSYS Fluent, captured for this research

Case 17 works with second order momentum equations and have same settings with case 5. The comparison of these two cases is an example of grid independence method. All

settings of them are the same, just the grid is different. Accordingly, case 17 gives the thrust force with 1.4680311 and this result becomes the lowest value in this study.

If each time step includes more than one revolution, more accurate results will be obtained. In case 18 and 19, the propeller rotates 10 revolutions at each time step. Both of them have second order momentum equations and case 19 has also second order turbulence kinetic energy and specific dissipation rate equations. Case 18 and case 19 have the thrust forces are 1.899773 N and 2.5080612 N, respectively. Figure 4.13 show the residuals of both case 18 and 19 are processed similarly. In addition, the velocity vectors are illustrated in Figure 4.14.

Figure 4.13: Residuals of case 18 and 19

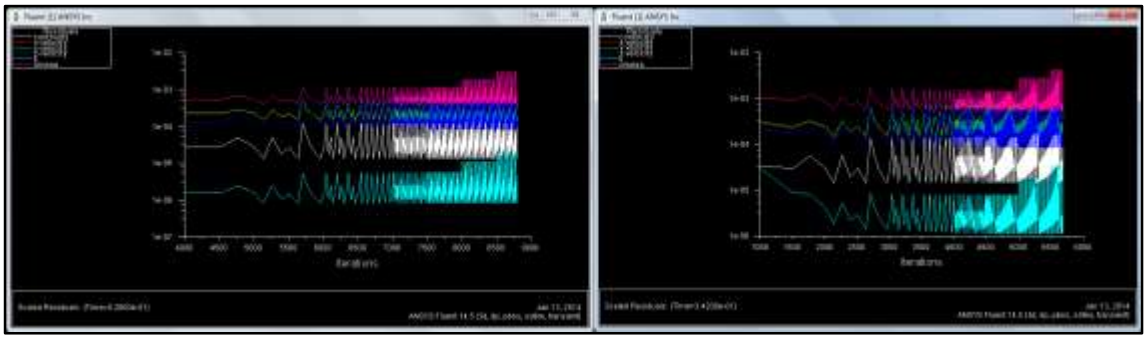

Source: a screenshot from ANSYS Fluent, captured for this research

Figure 4.14: Velocity vectors of case 18 and 19

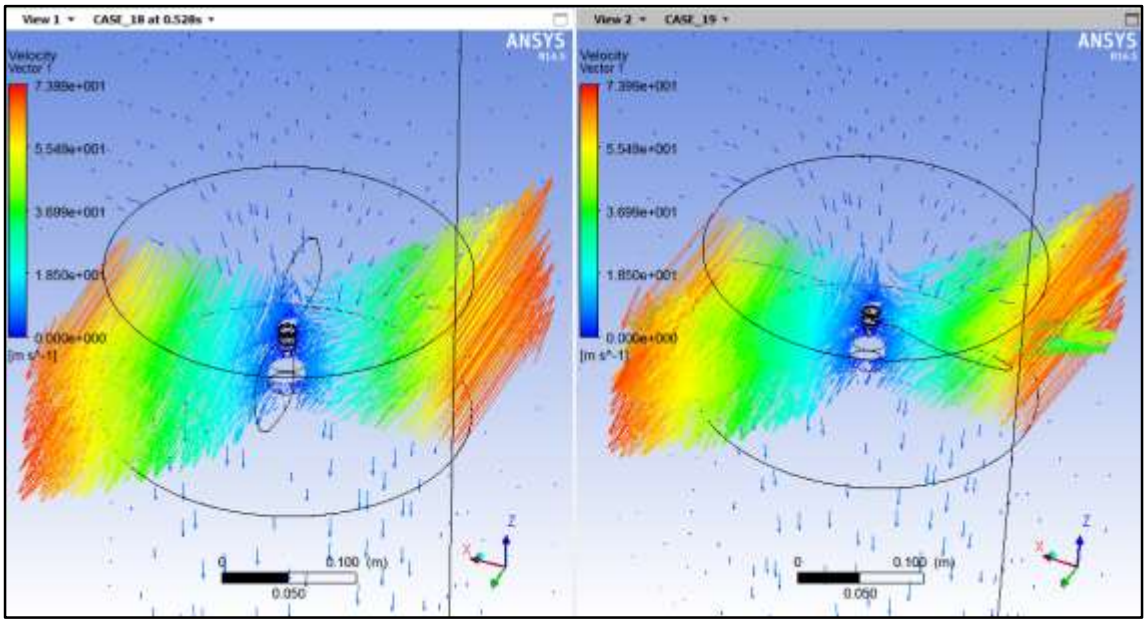

Source: a screenshot from ANSYS CFD-Post, captured for this research

4.3 PERIODIC HALF DOMAIN

This case is modelled in order to validate the results of both long and short computational domains. One blade of the propeller is formed with MRF method and it gives 1.0266519 N. That means one blade can generate this force. Therefore, in this case, the thrust force is obtained with 2.0533038 N validates most of other cases. Figure 4.15 indicates the residuals with 10000 iteration and the streamlines are illustrated in Figure 4.16.

Figure 4.15: Residual of periodic half domain

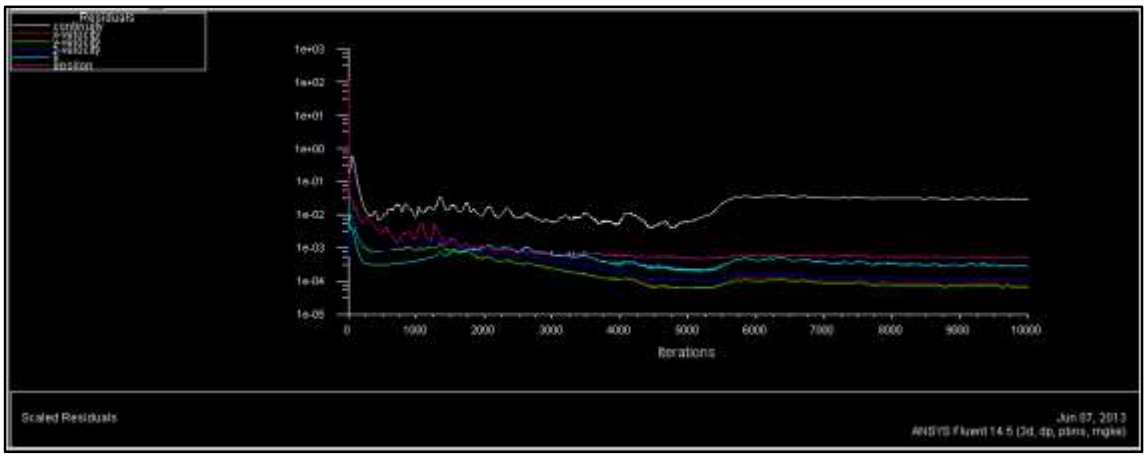

Source: a screenshot from ANSYS Fluent, captured for this research

Figure 4.16: The streamlines of the periodic half domain

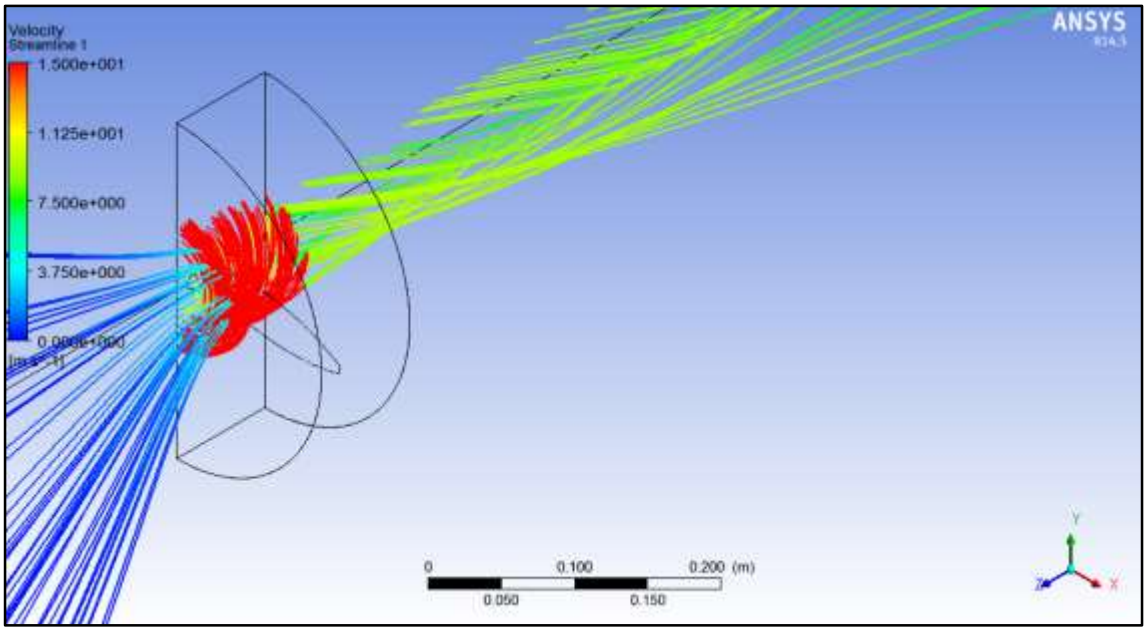

Source: a screenshot from ANSYS CFD-Post, captured for this research

4.4 QUADROTOR ITSELF

This is the final case after long and short domains and the periodic half case. The quarter quadrotor is modelled with symmetry BCs and solved with inviscid flow. The objective is the determination of the only lift force in this case with all quadrotor geometry.

Figure 4.17: Residuals of the quadrotor domain

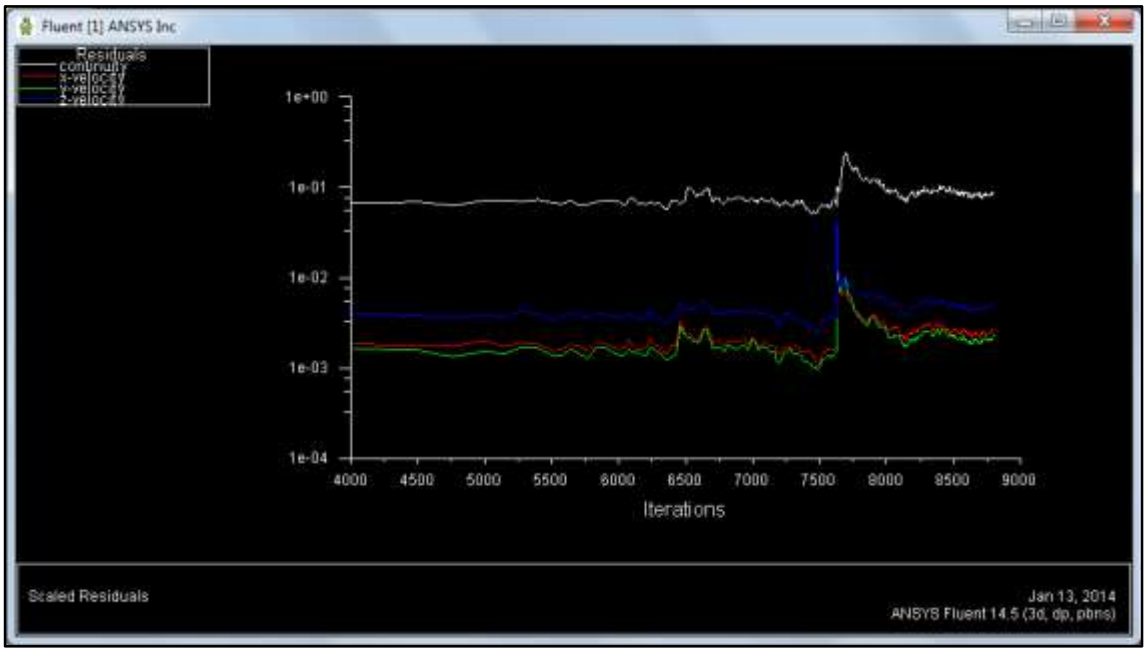

Source: a screenshot from ANSYS Fluent, captured for this research

Figure 4.18: Axial velocity contour of the quadrotor domain

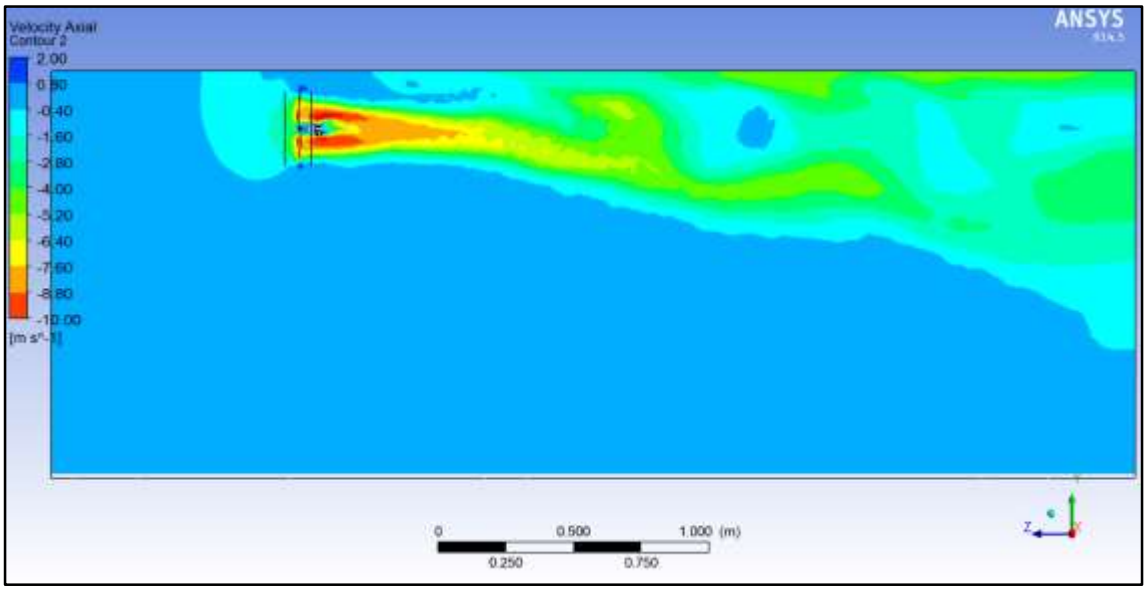

Source: a screenshot from ANSYS CFD-Post, captured for this research

There is no viscous force in this study. One rotor gives the thrust force with 2.0903624 N. That means quadrotor generates totally 8.3 N with lifting of 836.38496 g-force capacity. Figure 4.17, Figure 4.18, Figure 4.19 and Figure 4.20 show the residuals, axial velocity contours and streamlines, respectively.

Figure 4.19: Streamlines of the quadrotor domain

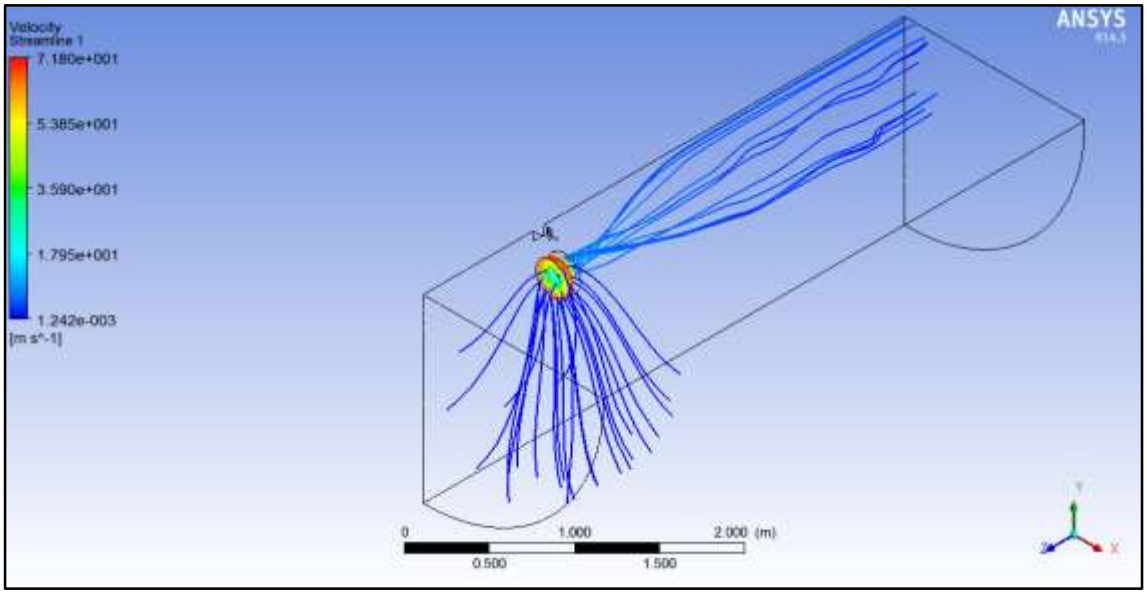

Source: a screenshot from ANSYS CFD-Post, captured for this research

Figure 4.20: Streamlines on all quadrotor geometry

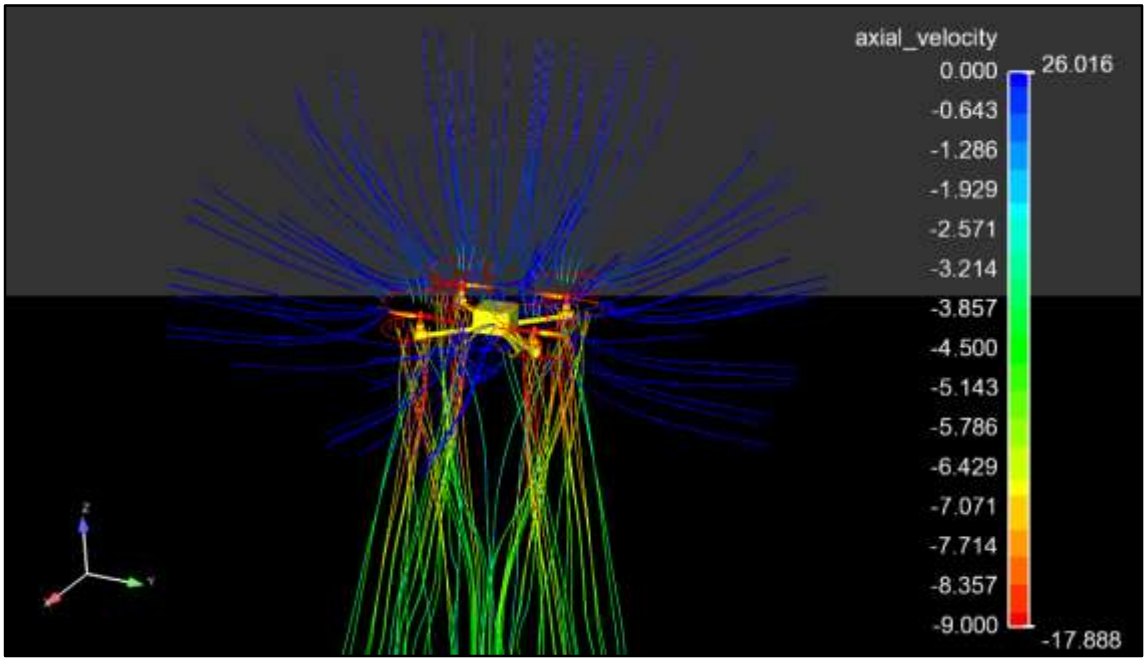

Source: a screenshot from Ensight GOLD, captured for this research

5. CONCLUSION & DISCUSSION

In this thesis, a model quadrotor, which is employed for hobby photography, is selected in order to make a CFD analysis. The objective is the simulation of the quadrotor at hover position and determination of the lift forces. Over 20 cases are run for this study and all of them are explained one by one with all specifications.

The computer capacity of this study is performed with 8 cores and up to 12 GB RAM. This capacity can solve a case with up to 6 million grid, any 2-eq RANS turbulence model and SIMPLE solution algorithm.

Two main computational domains are modelled with 5 different grids. All of them have different settings and each progression to next case is expressed in the previous chapters.

Firstly, the long solution domain is modelled with 15 m long in MRF method. That means the solution domain has two sub-domains. First one is the stationary domain which excludes the rotor and second one is the rotor domain which can rotate with frame motion option. Moreover, the patched interfaces of both sub-domains provides air flow easily. First five cases are solved as the long domain and case 4 and 5 give the logical results.

Secondly, the short solution domain is modelled with 4 m long and MRF method, too. Both long and short domains have nearly equal grid numbers. However, the cell sizes of the short domain grids are smaller than the long ones. That provides more quality results. Fifteen cases are solved as the short computational domain and twelve of them get more accurate results.

The right cases have similar settings, whereas they have just a few different options under the same method. For instance; the difference between case 6 and case 7 is only wall function type. Furthermore, case 8 is also similar to case 6 but case 8 works the different gradient evaluation option. In addition, case 9 has the same settings with case 8. However, the under-relaxation factors of case 9 is reduced. Case 13 is also solved with under-relaxation factors but the turbulence intensity option of the inlet BC is different from all true cases. Cases 10, 11, and 12 work with different viscous models; laminar, inviscid and low-Re k-eps, respectively. All true cases are listed in Table 5.1.

Table 5.1: The results of the true cases

Case	Thrust Force (N)
4	1,9474438
5	2,3393503
6	2,0379755
7	2,0253144
8	2,0531143
9	1,9933292
10	2,1197711
11	1,9536503
12	1,9023772
13	2,0024594
16	2,0328978
17	1,4680311
18	1,899773
19	2,5080612
Average	2,020253471

Source: formed by Excel with ANSYS Fluent settings

In addition, Table 5.1 shows the average thrust force is 2.02 N and standard deviation is 0.23 N.

The wrong results are obtained by selecting the wrong BCs. Cases 1 and 20 are tried with velocity inlet BC of 0 m/s but there is no accurate results. In addition, two more cases are solved to understand it the velocity inlet BC works sufficiently. Cases 2, 3 and 14 prove that the velocity inlet BC should run with an advance velocity. Moreover, case 15 is tried intake-fan BC for the propeller rotation. However, the selection of intake-fan is understood as a bad choice for the complex geometry.

After 20 cases, the validation case is modelled with periodic BC method. The propeller is divided by two through axial direction. The periodic half domain is solved with the same settings of case 8 and gives the thrust force is 2.0533038 N. This result has 0.02% error of case 8 and 1.2% error of the average result.

Finally, all quadrotor domain is modelled but it is solved with symmetrically. However, this case is just run as an inviscid flow since the lift force is generated by pressure levels and the drag forces caused by viscous flows are considered not necessary for this case.

This case gives the thrust force with 2.09 N has 3% error of average result. Accordingly, the quadrotor has 836.4 g lifting capacity and its own weight is approximately 1 kg.

The CFD results approach 16.4% error of its weight in this study since CFD algorithm has not robustness yet to solve a fan, a rotor or a propeller. If an airplane wing is imagined as one bladed rotor, CFD algorithms can solve the wake zone easily. However, rotors or propeller includes the blades that follow each other. After the present blade separates the flow, the next blade can meet the separated flow, not consolidated flow. This cause inefficient performance of propellers.

REFERENCES

Books

Tu J., Yeoh G. H., Liu C., 2007. *Computational Fluid Dynamics A Practical Approach.* Oxford: Butterworth-Heinemann

Versteeg H. K. & Malalasekera W., 1995. *An Introduction to Computational Fluid Dynamics - The Finite Volume Method*. England: Prentice Hall

Roy A., 2012. *A First Course on Aerodynamics*. BoBoCoAe, India: AR & Ventus Publishing ApS

Anderson J. D. Jr., 2001. Fundamentals of Aerodynamics – 3rd ed. New York: Mc Graw-Hill.

Journals

Anderson W. K. and Bonhaus D. L., 1994. An Implicit Upwind Algorithm for Computing Turbulent Flows on Unstructured Grids. *Computer Fluids*. **23** (1), pp. 1-21

Ambatipudi V., 2011. Simple Solver for Driven Cavity Flow Problem. *ASME*, pp. 1-8

Patankar S. V. and Spalding D. B., 1972. A Calculation Procedure for Heat, Mass and Momentum Transfer in Three Dimensional Parabolic Flows. *Int. J. of Heat and Mass Transfer*. **15** (10), pp. 1787-1806

Other publishing

Brandt J. B. and Selig M. S., 2011. Propeller Performance Data at Low Reynolds Numbers. AIAA Aerospace Sciences Meeting, 4-7 January 2011 Orlando, FL: American Institute of Aeronautics and Astronautics, pp. 1-18.